

2008

## A comparative study of silicon dioxide thin film deposition techniques and the fabrication of ultra-low refractive index nano-porous silicon dioxide thin film

Mengshu Pan  
*University of Dayton*

Follow this and additional works at: [https://ecommons.udayton.edu/graduate\\_theses](https://ecommons.udayton.edu/graduate_theses)

---

### Recommended Citation

Pan, Mengshu, "A comparative study of silicon dioxide thin film deposition techniques and the fabrication of ultra-low refractive index nano-porous silicon dioxide thin film" (2008). *Graduate Theses and Dissertations*. 4822.  
[https://ecommons.udayton.edu/graduate\\_theses/4822](https://ecommons.udayton.edu/graduate_theses/4822)

This Thesis is brought to you for free and open access by the Theses and Dissertations at eCommons. It has been accepted for inclusion in Graduate Theses and Dissertations by an authorized administrator of eCommons. For more information, please contact [mschlange1@udayton.edu](mailto:mschlange1@udayton.edu), [ecommons@udayton.edu](mailto:ecommons@udayton.edu).

**A COMPARATIVE STUDY OF SILICON DIOXIDE THIN FILM DEPOSITION  
TECHNIQUES AND THE FABRICATION OF ULTRA-LOW REFRACTIVE  
INDEX NANO-POROUS SILICON DIOXIDE THIN FILM**

**Thesis**

**Submitted to**

**The School of Engineering of the**

**UNIVERSITY OF DAYTON**

**In Partial Fulfillment of the Requirements for**

**The Degree**

**Master of Science in Electro-Optics**

**By**

**Mengshu Pan**

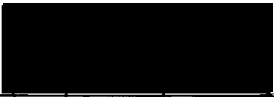
**UNIVERSITY OF DAYTON**


**Dayton, Ohio**

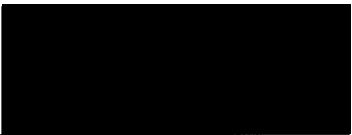
**August, 2008**

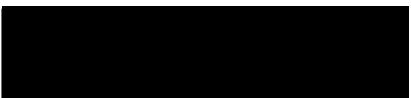
A COMPARATIVE STUDY OF SiO<sub>2</sub> THIN FILM DEPOSITION TECHNIQUES AND  
THE FABRICATION OF ULTRA-LOW REFRACTIVE INDEX NANO-POROUS SiO<sub>2</sub>  
THIN FILM

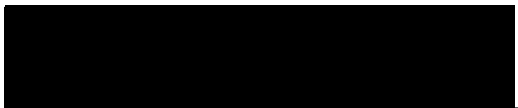
APPROVED BY:

  
\_\_\_\_\_  
Andrew Sarangan, Ph.D.  
Advisory Committee Chairman  
Associate Professor  
Electro-Optics Program

  
\_\_\_\_\_  
Joseph Haus, Ph.D.  
Committee Member  
Professor  
Electro-Optics Program

  
\_\_\_\_\_  
Qiwèn Zhan, Ph.D.  
Co-Advisor  
Associate Professor  
Electro-Optics Program

  
\_\_\_\_\_  
Malcolm W. Daniels, Ph.D.  
Associate Dean  
School of Engineering

  
\_\_\_\_\_  
Joseph E. Saliba, Ph.D., P.E.  
Dean, School of Engineering

## ABSTRACT

### A COMPARATIVE STUDY OF SILICON DIOXIDE THIN FILM DEPOSITION TECHNIQUES AND THE FABRICATION OF ULTRA-LOW REFRACTIVE INDEX NANO-POROUS SILICON DIOXIDE THIN FILM

Name: Pan, Mengshu  
University of Dayton

Advisor: Dr. A. M. Sarangan

$\text{SiO}_2$  thin films have many applications in modern electrical and optical engineering. Some unique properties of the  $\text{SiO}_2$  thin films and more importantly their interface with Si substrates make  $\text{SiO}_2$  one of the most important and studied materials in the field of microelectronics and optical devices.

This thesis presents a comparative analysis of three common methods to deposit  $\text{SiO}_2$  thin film on silicon substrates: Plasma Enhanced Chemical Vapor Deposition (PECVD), RF Plasma Sputtering and Electron-Beam (E-Beam) Evaporation. Film indices and thicknesses were characterized using a combination of ellipsometer and profilometer techniques. The effects of deposition process parameters on the  $\text{SiO}_2$  thin film indices in the 400nm to 900nm wavelength range and deposition rate were investigated and possible reasons were proposed. Finally, the deposition of a novel ultra-low refractive index nano-porous  $\text{SiO}_2$  thin film was demonstrated using oblique angle E-Beam Evaporation.

## ACKNOWLEDGEMENTS

I would like to thank Dr. Andrew Sarangan for his profound help and guidance with this thesis and throughout my graduate study. I would also like to thank Dr. Qiwen Zhan for his help and guidance especially in ellipsometry. Many thanks to Agus Widjaja, Emily Fehrman and Lirong Sun for their help during fabrication.

I am also very grateful to Electro-Optics Program, Dr. Joseph Haus, all other faculty members and Nancy Wilson.

Finally, I would like to thank my parents and my friends for their constant support to me.

## TABLE OF CONTENTS

ABSTRACT .....	iii
ACKNOWLEDGEMENTS .....	iv
LIST OF FIGURES .....	vii
CHAPTER	
I. SiO <sub>2</sub> THIN FILM APPLICATIONS AND FABRICATION METHODS .....	1
1.1 Applications of Thin Films .....	1
1.2 Applications of SiO <sub>2</sub> Thin Films .....	1
1.3 Important Parameters of SiO <sub>2</sub> Thin Films .....	2
1.4 Fabrication of SiO <sub>2</sub> Thin Films .....	4
II. SiO <sub>2</sub> THIN FILM DEPOSITION USING PLASMA ENHANCED CHEMICAL VAPOR DEPOSITION .....	6
2.1 Introduction to Plasma Enhanced Chemical Vapor Deposition .....	6
2.2 Effects of PECVD Process Parameters on SiO <sub>2</sub> Thin Films .....	9
2.2.1 Effects of Gases Flow Ratio on SiO <sub>2</sub> Thin Films .....	9
2.2.2 Effects of Substrate Temperature on SiO <sub>2</sub> Thin Films .....	14
2.2.3 Effects of Process Pressure on SiO <sub>2</sub> Thin Films .....	16
2.2.4 Effects of RF Power on SiO <sub>2</sub> Thin Films .....	17
2.3 Features of Thin Films Deposited by Plasma Enhanced Chemical Vapor Deposition .....	20
2.4 Gas Contamination in Plasma Enhanced Chemical Vapor Deposition .....	20
III. SiO <sub>2</sub> THIN FILM DEPOSITION USING RF PLASMA SPUTTERING .....	22
3.1 Introduction to RF Plasma Sputtering .....	22
3.2 Effects of RF Sputtering Process Parameters on SiO <sub>2</sub> Thin Films .....	25
3.2.1 Effects of Process Pressure on SiO <sub>2</sub> Thin Films .....	25
3.2.2 Effects of RF Power on SiO <sub>2</sub> Thin Films .....	27
3.2.3 Effects of Sputter Angle on SiO <sub>2</sub> Thin Films .....	28
3.3 Features of Thin Films Deposited by RF Sputtering .....	30
IV. SiO <sub>2</sub> THIN FILM DEPOSITION USING ELECTRON-BEAM EVAPORATION ..	31

4.1 Introduction to Electron-Beam Evaporation.....	31
4.2 Effects of Evaporation Angle on SiO <sub>2</sub> Thin Films .....	33
4.3 Features of Thin Films Deposited by Electron-Beam Evaporation.....	33
 V. ULTRA-LOW REFRACTIVE INDEX NANO-POROUS SiO <sub>2</sub> THIN FILM FABRICATION.....	 35
5.1 Applications of Ultra-Low Refractive index Nano-Porous SiO <sub>2</sub> Thin Films .....	35
5.2 Fabrication of Ultra-Low Refractive index Nano-Porous SiO <sub>2</sub> Thin Films .....	35
 VI. ELLIPSOMETRY .....	 42
6.1 Introduction to Ellipsometry .....	42
6.2 SiO <sub>2</sub> Characterization Using Ellipsometry .....	43
 VII. CONCLUSIONS .....	 46
 BIBLIOGRAPHY .....	 47

## LIST OF FIGURES

<b>Figure 1</b> (a) Schematic illustration of PECVD process. (b) Unaxis 790 Series Plasma Processing System.....	7
<b>Figure 2</b> (a) Chamber inside view. (b) Chamber with plasma on. ....	8
<b>Figure 3</b> Refractive index of PECVD SiO <sub>2</sub> thin film vs. wavelength at different flow ratio (0~4). ....	11
<b>Figure 4</b> Refractive index of PECVD SiO <sub>2</sub> thin film vs. wavelength at different flow ratio (0.25~4). ....	12
<b>Figure 5</b> Refractive index of PECVD SiO <sub>2</sub> thin film vs. flow ratio at different wavelengths.....	12
<b>Figure 6</b> Deposition rate of PECVD SiO <sub>2</sub> thin film vs. flow ratio.....	13
<b>Figure 7</b> Refractive index of PECVD SiO <sub>2</sub> thin film vs. wavelength at different substrate temperature. ....	14
<b>Figure 8</b> Deposition rate of PECVD SiO <sub>2</sub> thin film vs. substrate temperature.....	15
<b>Figure 9</b> Refractive index of PECVD SiO <sub>2</sub> thin film vs. wavelength at different process pressure. ....	16
<b>Figure 10</b> Deposition rate of PECVD SiO <sub>2</sub> thin film vs. process pressure.....	17
<b>Figure 11</b> Refractive index of PECVD SiO <sub>2</sub> thin film vs. wavelength at different RF power.....	18
<b>Figure 12</b> Refractive index of PECVD SiO <sub>2</sub> thin film vs. wavelength at high and low RF power.....	18
<b>Figure 13</b> Deposition rate of PECVD SiO <sub>2</sub> thin film vs. RF power. ....	19
<b>Figure 14</b> Testing results for gas contamination in PECVD SiO <sub>2</sub> thin film caused by leak in gas lines.....	21



<b>Figure 15</b> (a) Schematic illustration of RF sputtering. (b) Denton Vacuum RF Sputtering tool.....	23
<b>Figure 16</b> (a) Denton chamber in use. (b) SiO <sub>2</sub> target for sputtering .....	23
<b>Figure 17</b> Cross section of the magnet configuration for a magnetron cathode. ....	24
<b>Figure 18</b> Refractive index of RF sputtered SiO <sub>2</sub> thin film vs. wavelength at different process pressure. ....	26
<b>Figure 19</b> Deposition rate of RF sputtered SiO <sub>2</sub> thin film vs. process pressure .....	27
<b>Figure 20</b> Deposition rate of RF sputtered SiO <sub>2</sub> thin film vs. RF power.....	28
<b>Figure 21</b> Experiment setup for oblique angle sputtering.....	29
<b>Figure 22</b> Refractive index of RF sputtered SiO <sub>2</sub> thin film vs. wavelength at different sputter angles.....	29
<b>Figure 23</b> (a) Schematic illustration of E-Beam evaporation process. (b) International Torr Electron-Beam evaporator.....	32
<b>Figure 24</b> (a) SiO <sub>2</sub> source pellets. (b) Graphite crucible used for SiO <sub>2</sub> evaporation. (c) SiO <sub>2</sub> in crucible after evaporation. ....	33
<b>Figure 25</b> Schematic illustration of oblique angle E-Beam evaporation. ....	36
<b>Figure 26</b> Experiment setup of oblique angle E-Beam evaporation. ....	36
<b>Figure 27</b> (a) Adjustable angle fixture used in oblique angle evaporation. (b) Samples ready for oblique angle evaporation. ....	37
<b>Figure 28</b> SiO <sub>2</sub> nano-rods layer evaporated at 80°.....	37
<b>Figure 29</b> Ti nano-rods layer evaporated at 80°.....	38
<b>Figure 30</b> Ag film evaporated at 80°.....	39
<b>Figure 31</b> Surface sealing step in E-Beam oblique angle evaporation. ....	39
<b>Figure 32</b> Refractive index of E-Beam evaporated SiO <sub>2</sub> thin film vs. wavelength at different evaporation angle .....	40
<b>Figure 33</b> Refractive index of E-Beam evaporated SiO <sub>2</sub> thin film vs. wavelength at different measurement orientations.....	41

<b>Figure 34</b> PhE-102 spectroscopic Ellipsometer.....	43
<b>Figure 35</b> Ellipsometer fitting curves of $\Psi$ and $\Delta$ .....	44

## CHAPTER I

### SiO<sub>2</sub> THIN FILM APPLICATIONS AND FABRICATION METHODS

#### 1.1 Applications of Thin Films

Thin films range in thickness from a few angstroms to a few thousand angstroms deposited on suitable substrates to achieve properties unattainable or not easily attainable in the bulk form [1]. Electronic semiconductor devices and optical coatings are two main applications of thin films, but thin films are used in virtually all aspects of modern life ranging from decorative paint coatings, anti-corrosion coatings to TiN hardness coating of machine tools and medical devices. Thin film materials range from ceramics, semiconductors and metals to complex polymers and nano-particles.

#### 1.2 Applications of SiO<sub>2</sub> Thin Films

The primary application of SiO<sub>2</sub> thin films is as an electrical gate insulation film in silicon integrated transistors, which are the overwhelming majority of electronic devices used in the present day [2]. This specific application cannot be accomplished to the required precision and cost with any other materials except SiO<sub>2</sub>.

In addition, SiO<sub>2</sub> thin films have other important functions within silicon micro-electronics such as for electrical isolation between devices on a densely populated chip and between different layers of metal interconnects, as a masking film for chemical etching, for packaging and for MEMS research. More recently, Silicon-on-Insulator (SOI)

technology has emerged as an alternative to bulk silicon, which utilizes a thin layer of  $\text{SiO}_2$  to isolate the electronic components from the substrate for improved performance.

In addition to microelectronics,  $\text{SiO}_2$  thin films are also widely used in optical coatings as the low refractive index layers. In multilayer structures, the relatively low refractive index of  $\text{SiO}_2$  thin film, in combination with another higher refractive index material can create a large refractive index contrast, which is a key figure of merit in many applications, such as dielectric multilayer structures, optical resonators and photonic crystals. There are only a handful of materials with refractive index lower than  $\text{SiO}_2$ , and none of them can be produced as cheaply as  $\text{SiO}_2$ . Hence, there is interest in producing  $\text{SiO}_2$  thin films with indices lower than their bulk values. In this thesis, a novel technique was utilized to successfully produce nano-structured  $\text{SiO}_2$  thin films with ultra-low refractive indices. This will be described in detail in Chapter V.

### 1.3 Important Parameters of $\text{SiO}_2$ Thin Films

Although  $\text{SiO}_2$  is generally referred to as “silica glass”, there are literally hundreds of different types of silica obtained with different impurity levels which have distinct optical and mechanical properties. Even in its pure form,  $\text{SiO}_2$  exhibits different properties depending on the deposition technique and deposition parameters. Therefore, a careful analysis of each type of thin film after deposition is required. At the same time emphasis has been placed on the process parameters in order to have additional control and to gain a better understanding of the process, which will be discussed in detail in subsequent chapters on the different deposition techniques. The results of the analyses are then used to adjust the conditions for film property modification.

A few important parameters of  $\text{SiO}_2$  thin films include refractive index, packing density, uniformity, surface roughness and step-coverage. Refractive index is the most fundamental quantity of interest in optical sciences. The refractive index of a medium determines not only the phase velocity of light, but also more importantly, the refraction, reflection and diffraction occurring at the boundaries of the medium. The precise control of the refractive indices of  $\text{SiO}_2$  thin films is of great importance for a large set of optical devices including antireflection coatings, interference filters, waveguides and other similar applications. The refractive index is an indication of film packing density, which is another important parameter of thin films. Thin films with lower packing density will also have lower refractive indices, and this principle is used to fabricate the ultra-low refractive index  $\text{SiO}_2$  thin films. However, thin films with low packing density will have compromised mechanical properties and a greater chemical sensitivity to the environment. They will also absorb environmental moisture, leading to variations in performance. Despite their weaknesses, these properties could also have potential applications in environmental sensors.

Step-coverage, also known as conformality is of great interest in microelectronic industry. It describes how well a thin film covers a morphologically uneven interface. In lift-off patterning applications, the thin film should ideally be non-conformal to allow a path for the etching solvents to attack the sacrificial layer. In passivation and planarization applications, a conformal thin film is desired, which means the thin film should coat all structural areas of the substrate including steep walls, and not just the top surface areas. Different deposition methods can produce quite different degrees of step-coverage.

Deposition rate of thin films describes how fast the thin films grow. It is one of the important concerns in manufacturing production. Deposition rate can also affect the film quality. Compared with high deposition rate, lower deposition rate tend to produce thin films with higher uniformity and density.

Refractive indices and deposition rate of  $\text{SiO}_2$  thin films produced by different deposition methods were investigated and data was presented in this thesis.

#### 1.4 Fabrication of $\text{SiO}_2$ Thin Films

Thin film deposition process is a sequence of several steps [1]. The material is extracted from the source and transported to the substrate, deposition takes place, sometimes annealing is applied afterwards, and finally the thin film is characterized to evaluate the process.

The source materials of  $\text{SiO}_2$  thin films can be a solid  $\text{SiO}_2$  target or pellets, or its constituent gases. Solid source materials need to be vaporized to be transported to the substrate and condense on it to form a layer of thin film. This can be done by ion bombardment in plasma (sputtering) or energetic electron beam (E-Beam evaporation). These methods are categorized as physical vapor deposition (PVD). In other cases, the source material is supplied as reactive gases ( $\text{N}_2\text{O}$  and diluted  $\text{SiH}_4$  in this thesis) at certain vapor pressure to be transported at moderate temperature. Deposition processes that use gases, evaporating liquids or chemically gasified solids as the precursor materials to a chemical reaction are categorized as chemical vapor deposition (CVD). Plasma can be applied to assist the chemical reaction between the precursors and allow it to occur at

lower substrate temperature compared with conventional CVD. This is referred as plasma enhanced CVD (PECVD).

Thermal oxidization is used in applications where the highest quality  $\text{SiO}_2$  thin films are required, such as integrated electronic devices. These  $\text{SiO}_2$  thin films are produced by direct oxidation of the silicon substrate in a pure oxygen or water vapor ambient at elevated temperature. Thermal oxide layers cannot be made very thick because the oxygen cannot penetrate very deep below the substrate surface, and the resulting  $\text{Si}/\text{SiO}_2$  interface will be diffused. For these reasons, although it is the highest quality oxide, thermal oxide is rarely used in optical thin film applications.

PECVD, RF sputtering and E-Beam evaporation will be discussed in details in following chapters. Thermal oxidization is not part of this thesis.

## CHAPTER II

### SiO<sub>2</sub> THIN FILM DEPOSITION USING PLASMA ENHANCED CHEMICAL VAPOR DEPOSITION

#### 2.1 Introduction to Plasma Enhanced Chemical Vapor Deposition

CVD is a material synthesis process whereby constituents of the vapor phase react chemically near or on a substrate surface to form a solid product of thin film. The use of CVD technology has become one of the most important means for creating thin films essential to advanced technology, particularly solid-state electronics where some of the most sophisticated composition requirements must be met. The theory of CVD is based on chemical kinetics, fluid mechanics, chemical engineering principles, and an understanding of growth mechanisms.

A number of forms of CVD are widely in use. These processes differ in the way of activation process and process conditions. APCVD, LPCVD and PECVD are three most common forms of CVD.

APCVD is atmospheric-pressure CVD, which operates at atmospheric pressure as its name refers. The reactor designs are simple, yet provide high deposition rate.

LPCVD is low-pressure CVD, which operates at sub-atmospheric pressure. Reduced pressure tend to reduce the particle contamination caused by unwanted gas-phase reactions and improve film quality in purity, uniformity and conformality, but with lower deposition rate.



In PECVD (plasma enhanced CVD), the chemical reactions take place in a plasma, which allows a lower substrate temperature than would be possible without a plasma. Low temperature processing is often critical in the manufacture of many sensitive electronics and optoelectronics. High energy ions from a plasma discharge break the bonds of the precursor molecules creating a large number of free radicals and allow the reaction to occur easier [3]. The ion bombardment on the substrate surface improves the adhesion and denser films are obtained. With the ability to vary the input energy to the reactor via the RF used to generate the plasma, the deposition rate, and to some extent, the film properties can be optimized. The number of process parameters makes PECVD a complex process but they also allow a large degree of control over the thin film properties. The schematic illustration of the PECVD process is shown in Fig. 1(a).

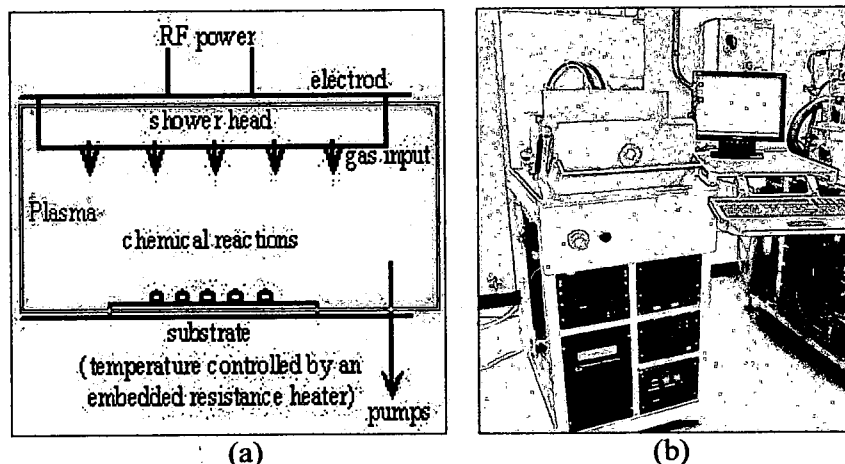


**Figure 1** (a) Schematic illustration of PECVD process. (b) Unaxis 790 Series Plasma Processing System.

The PECVD tool used for  $\text{SiO}_2$  thin film deposition in this thesis is Unaxis 790 Series Plasma Processing System as shown in Fig. 1(b). It contains the RF generator and matching network, power distribution circuitry, fluid distribution panel, gas handling system, vacuum connection, and the control computer [4].

Fig. 2(a) shows the inside view of the chamber, which contains two parallel electrode plates. The top plate is powered by RF and has tiny gas delivery holes in a shower head arrangement. The bottom plate is grounded, and also serves as a temperature controlled hot plate. The reddish color is silicon residues from previous silicon-rich deposition runs. The chamber can be cleaned by running  $\text{SF}_6$  flow for 30 minutes at 60sccm, making use of the strong etching effect of  $\text{SF}_6$  on Si. Fig. 2(b) is the photo through the view port when the plasma is on.

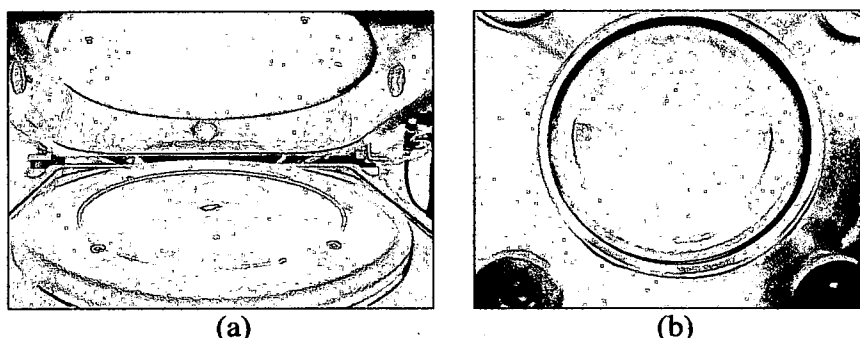
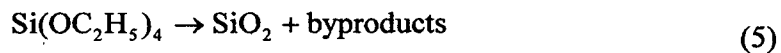
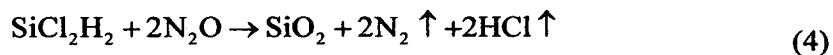
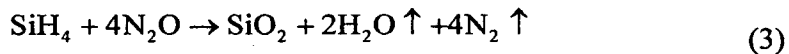
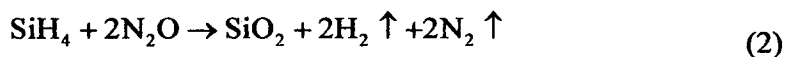
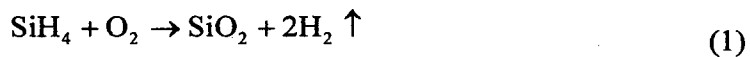


Figure 2 (a) Chamber inside view. (b) Chamber with plasma on.

$\text{SiO}_2$  thin films can be deposited by PECVD using several different precursors. Common source gases include  $\text{SiH}_4$  and  $\text{O}_2/\text{N}_2\text{O}$ ,  $\text{SiCl}_2\text{H}_2$  (dichlorosilane) and  $\text{N}_2\text{O}$ , or TEOS ( $\text{Si}(\text{OC}_2\text{H}_5)_4$ , tetraethylorthosilicate). The reactions can be as follows:



In this thesis,  $\text{N}_2\text{O}$  and 2% diluted  $\text{SiH}_4$  (remainder He) were used to deposit  $\text{SiO}_2$  thin films. As  $\text{SiH}_4$  reacts with  $\text{N}_2\text{O}$ ,  $\text{SiO}_2$  is formed and condenses on the substrate as a layer of thin film, while the byproducts  $\text{N}_2$ ,  $\text{H}_2$  and/or  $\text{H}_2\text{O}$  are pumped out of the chamber. The reason for  $\text{N}_2\text{O}$  instead of  $\text{O}_2$  is that  $\text{O}_2$  will react too fast and too spontaneously with  $\text{SiH}_4$ , creating  $\text{SiO}_2$  powder during the transport phase in the delivery tubes before they reach the substrate, while  $\text{N}_2\text{O}$  has a lower reactivity with  $\text{SiH}_4$  until the gases enter the plasma discharge.

## 2.2 Effects of PECVD Process Parameters on $\text{SiO}_2$ Thin Films

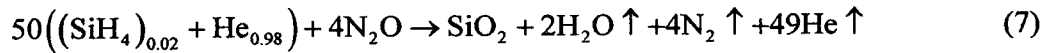
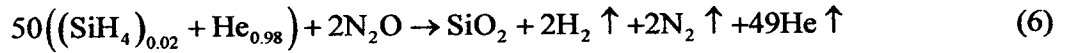
PECVD process variables such as substrate temperature, process pressure, input concentrations and gas flow rate determine the deposition rate and other properties of the thin film. In order to have a better understanding and control over the properties of the consequent thin film, the influences of gases flow ratio, substrate temperature, process pressure and RF power on refractive indices and deposition rate of  $\text{SiO}_2$  thin films were investigated in following sections.

### 2.2.1 Effects of Gases Flow Ratio on $\text{SiO}_2$ Thin Films

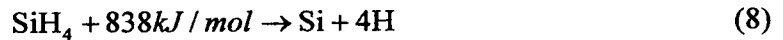
$\text{N}_2\text{O}/(\text{SiH}_4\&\text{He})$  flow ratio has the greatest influence on the refractive index of the deposited  $\text{SiO}_2$  thin films. With the variation of  $\text{N}_2\text{O}/(\text{SiH}_4\&\text{He})$  from 0 to 4 and above, Si,  $\text{SiO}_x$  ( $0 < x < 2$ ) and  $\text{SiO}_2$  thin films can be produced. By varying the  $\text{N}_2\text{O}/(\text{SiH}_4\&\text{He})$  flow ratio, we can obtain  $\text{SiO}_x$  thin films with varying refractive indices.

The gas flow is controlled by a mass flow controller (MFC), which functions by measuring the temperature difference in the flow stream at two different points due to a

fixed heating element. This temperature difference is a measure of the molecular mass which can then be converted to the commonly used unit of *standard cubic centimeters per minute* (sccm). A highly diluted mixture of 2% SiH<sub>4</sub> and 98% He was used instead of pure SiH<sub>4</sub> for safety reason because SiH<sub>4</sub> is pyrophoric (it spontaneous reacts exothermically with ambient air without the need for external ignition). So Eq.2 and Eq.3 can be written as:



The N<sub>2</sub>O/(SiH<sub>4</sub>&He) flow ratio in Eq.6 and Eq.7 is much lower than what were used in this thesis. This is because N<sub>2</sub>O is much more difficult to dissociate into free radicals than SiH<sub>4</sub>. SiH<sub>4</sub> has an enthalpy of formation of 34kJ/mol from its constituents Si and H<sub>2</sub>, and H has an enthalpy of formation of 218kJ/mol. As a result, it takes 838kJ/mol to dissociate SiH<sub>4</sub> into Si and H free radicals:



Likewise, N<sub>2</sub>O has an enthalpy of formation of 82kJ/mol from its constituents N<sub>2</sub> and O<sub>2</sub>. N has an enthalpy of formation of 472kJ/mol, and O has an enthalpy of formation of 250kJ/mol. As a result, it takes 1112kJ/mol to dissociate N<sub>2</sub>O into N and O free radicals:



The activation energy needed for N<sub>2</sub>O to satisfy Eq.2 or Eq.3 is much higher than for SiH<sub>4</sub>. Therefore, only a small fraction of N<sub>2</sub>O will be reactive, and a higher N<sub>2</sub>O/(SiH<sub>4</sub>&He) flow ratio was used at 25W RF power.

Refractive indices of SiO<sub>2</sub> thin films deposited by PECVD as a function of wavelength at different N<sub>2</sub>O/(SiH<sub>4</sub>&He) flow ratio are shown in Fig. 3 below.

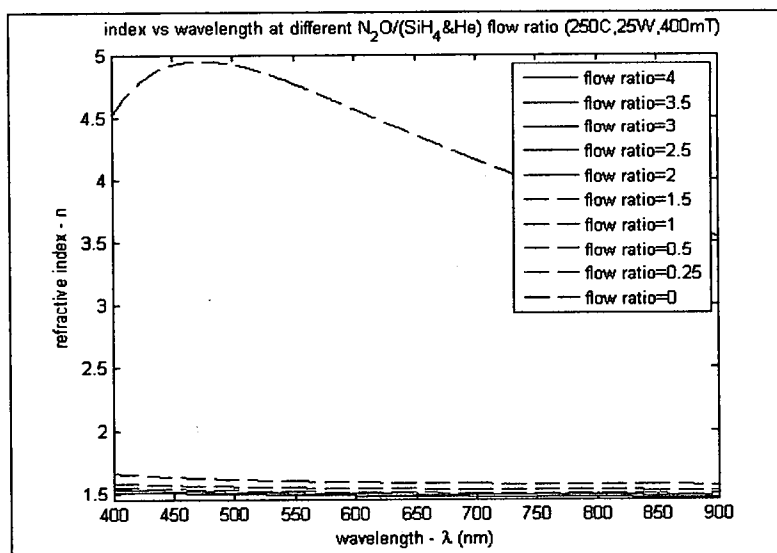


**Figure 3** Refractive index of PECVD  $SiO_2$  thin film vs. wavelength at different flow ratio (0~4).

When the  $N_2O/(SiH_4\&He)$  flow ratio is lowered down to zero, the  $SiO_2$  thin film had a much higher refractive index of 3.5 than under other  $N_2O/(SiH_4\&He)$  flow ratio, which were around 1.5. This is as expected because when  $N_2O/(SiH_4\&He)$  flow ratio is zero, the deposition would be pure silicon, the refractive index of which is 3.5, while under other  $N_2O/(SiH_4\&He)$  flow ratio, the product is silicon dioxide or silicon monoxide with refractive index around 1.5. The experimental result confirms the theory.

Fig. 4 below shows the part for the  $N_2O/(SiH_4\&He)$  flow ratio from 0.25 to 4.

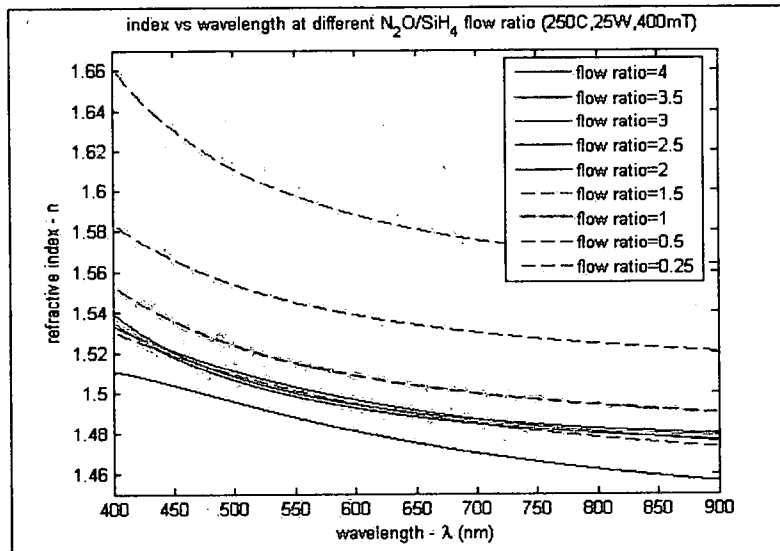


Figure 4 Refractive index of PECVD SiO<sub>2</sub> thin film vs. wavelength at different flow ratio (0.25~4).

Fig. 5 below shows the influences of the N<sub>2</sub>O/(SiH<sub>4</sub>&He) flow ratio from 0.25 to 4 on the refractive index of SiO<sub>2</sub> thin film deposited by PECVD at different wavelengths.

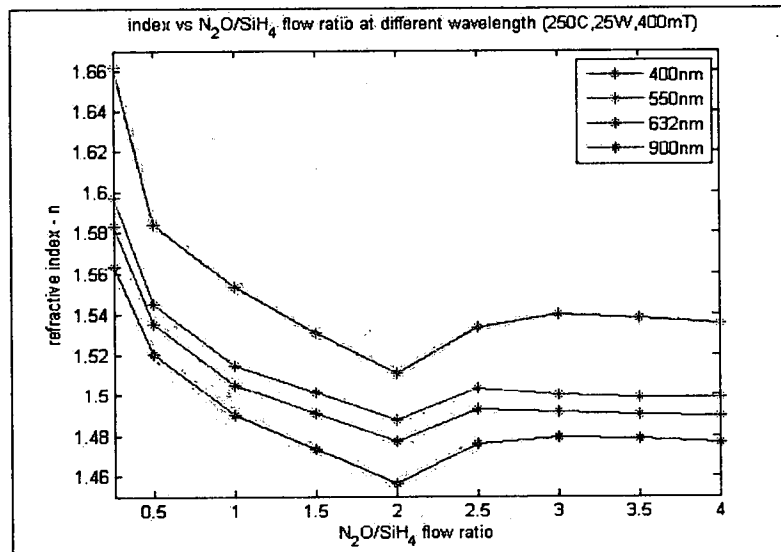


Figure 5 Refractive index of PECVD SiO<sub>2</sub> thin film vs. flow ratio at different wavelengths.

With increasing N<sub>2</sub>O/(SiH<sub>4</sub>&He) flow ratio, the indices first decreased, reached the lowest point at N<sub>2</sub>O/(SiH<sub>4</sub>&He) flow ratio=2, then increased a little, finally reached a steady state and did not change much after N<sub>2</sub>O/(SiH<sub>4</sub>&He) flow ratio=2.5. The decrease

of refractive index at first is as expected because of the decrease of Si and increase of SiO<sub>2</sub> content in the thin film. Two regimes are recognized here. The source gases flow ratio limited regime occurs at lower flow ratio, and the substrate surface reaction limited regime occurs at higher flow ratio.

Fig. 6 below shows the influence of the N<sub>2</sub>O/(SiH<sub>4</sub>&He) flow ratio on the deposition rate of SiO<sub>2</sub> thin film deposited by PECVD.

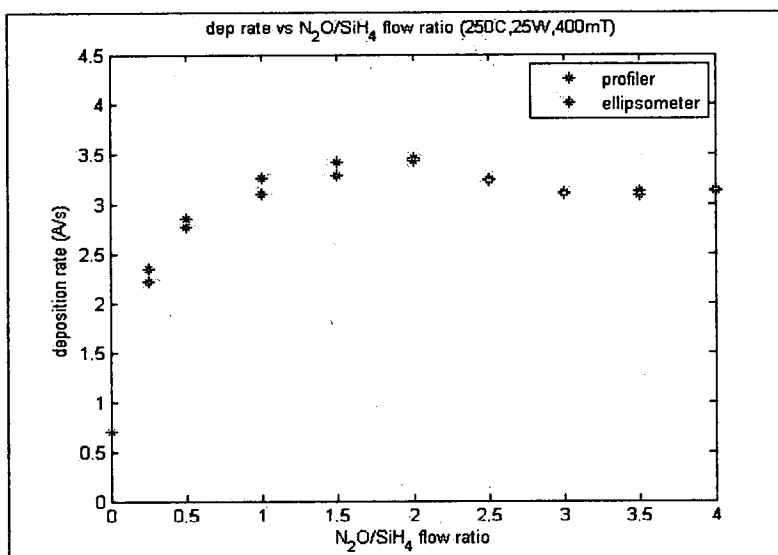


Figure 6 Deposition rate of PECVD SiO<sub>2</sub> thin film vs. flow ratio.

With increasing N<sub>2</sub>O/(SiH<sub>4</sub>&He) flow ratio, the deposition rate first increased, reached the highest point at N<sub>2</sub>O/(SiH<sub>4</sub>&He) flow ratio=2, then decreased a little, finally reached a steady state and did not change much beyond N<sub>2</sub>O/(SiH<sub>4</sub>&He) flow ratio=2.5. The trend of the curve corresponded to the refractive index change vs. N<sub>2</sub>O/(SiH<sub>4</sub>&He) flow ratio. The increment at first is attributed to the decrease of Si and increase of SiO<sub>2</sub> content in the thin film, and SiO<sub>2</sub> has a much higher deposition rate than Si. Again, two regimes are recognized here. The deposition was source gases flow ratio limited at low

flow ratio, and become substrate surface reaction limited after  $\text{N}_2\text{O}/(\text{SiH}_4\&\text{He})$  flow ratio=2.5.

### 2.2.2 Effects of Substrate Temperature on $\text{SiO}_2$ Thin Films

Substrate temperature is a major factor that affects properties of the  $\text{SiO}_2$  thin films deposited by PECVD. Refractive indices of  $\text{SiO}_2$  thin films deposited by PECVD as a function of wavelength at different substrate temperature are shown in Fig. 7 below.

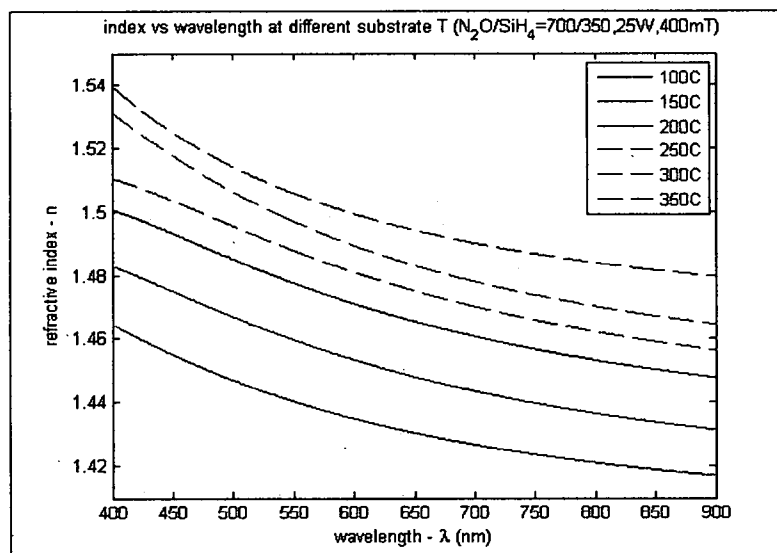


Figure 7 Refractive index of PECVD  $\text{SiO}_2$  thin film vs. wavelength at different substrate temperature.

With increasing substrate temperature, the index increased consistently. This kind of behavior can be explained by the changes in  $\text{SiO}_2$  thin film density. When the substrate temperature is increased, the thermal motions of the molecules deposited on the substrate surface will be greater, leading to a denser layer of  $\text{SiO}_2$  thin film, and result in higher refractive index. Another possible reason is that with the increasing substrate temperature, a stronger out gassing of oxygen could result in a higher Si content in the resultant thin



film. Since Si has a relative high refractive index, the overall refractive index of the thin film increased.

Fig. 8 below shows the influence of the substrate temperature on the deposition rate of SiO<sub>2</sub> thin film deposited by PECVD.

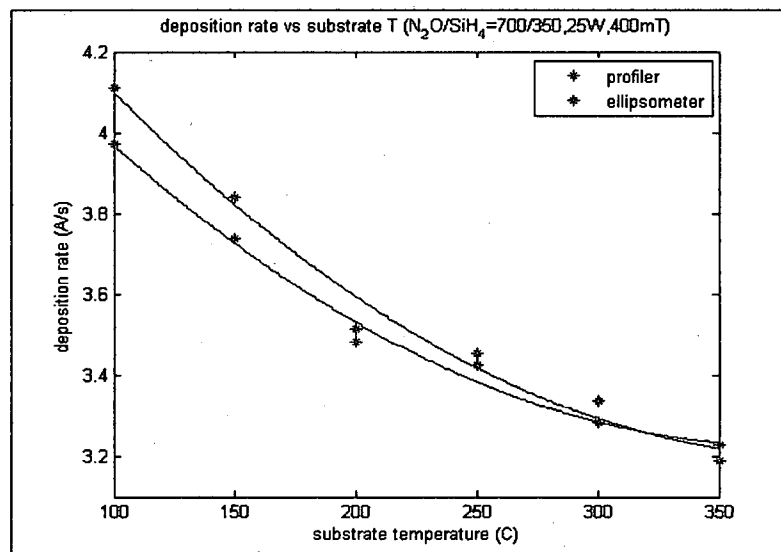


**Figure 8** Deposition rate of PECVD SiO<sub>2</sub> thin film vs. substrate temperature.

With increasing substrate temperature, the deposition rate was found to decrease. This behavior can be explained by the greater thermal motion of the surface atoms which could repel the condensation of the SiO<sub>2</sub> from the plasma. Another possible reason is that with the increasing substrate temperature, the Si content in the deposited film is increased. Since Si has a relative low deposition rate, the overall deposition rate of the resulting film decreased.

### 2.2.3 Effects of Process Pressure on SiO<sub>2</sub> Thin Films

Effect of process pressure on SiO<sub>2</sub> thin film index is yet unclear from our experiments. Fig. 9 below shows the refractive index of SiO<sub>2</sub> thin film deposited by PECVD as a function of wavelength at different process pressure.

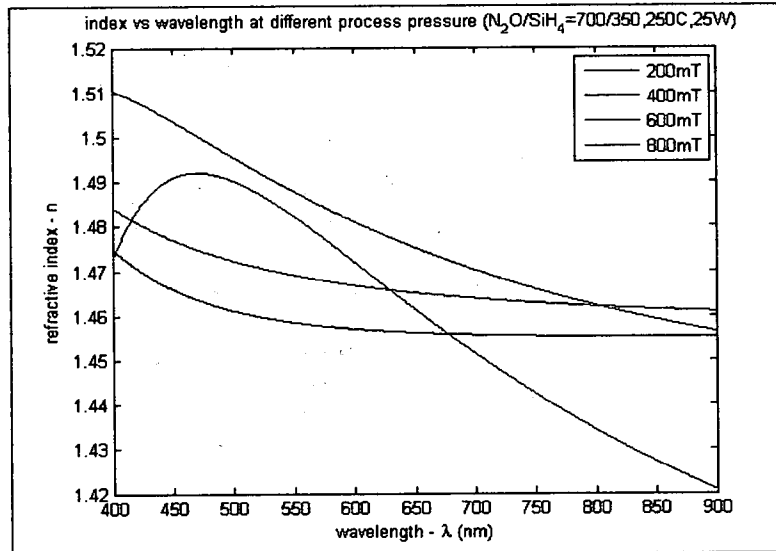


Figure 9 Refractive index of PECVD SiO<sub>2</sub> thin film vs. wavelength at different process pressure.

Fig. 10 below shows the influence of the process pressure on the deposition rate of SiO<sub>2</sub> thin film deposited by PECVD.

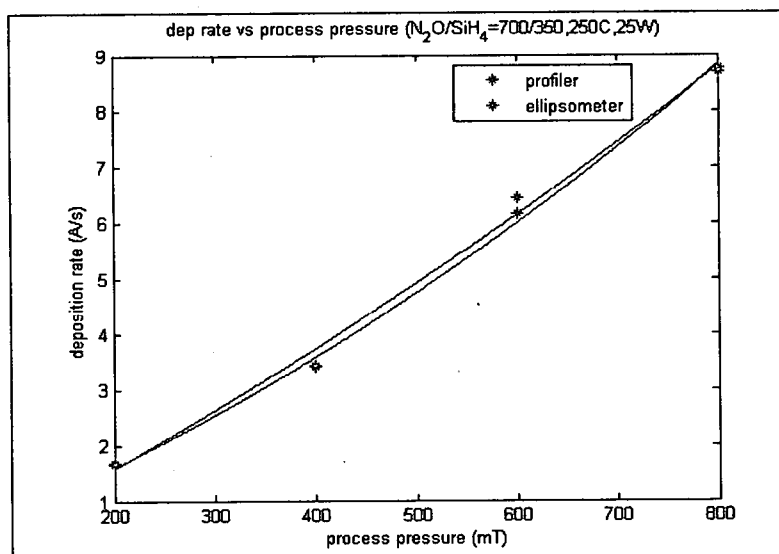


Figure 10 Deposition rate of PECVD SiO<sub>2</sub> thin film vs. process pressure.

The increase in the deposition rate with increasing process pressure is as expected. Higher process pressure means more reactive precursors in the chamber at the fixed plasma excitation power. Compared with lower process pressure, more free radicals will be present at higher process pressure, which lead to a higher deposition rate. From the experiments, we found that the process pressure had the greatest influence on the SiO<sub>2</sub> thin film deposition rate compared with other process parameters.

#### 2.2.4 Effects of RF Power on SiO<sub>2</sub> Thin Films

Parameters for PECVD SiO<sub>2</sub> thin films can be controlled through varying the plasma-sustaining RF power. Refractive index of SiO<sub>2</sub> thin film deposited by PECVD as a function of wavelength at different RF power is shown in Fig. 11 below.

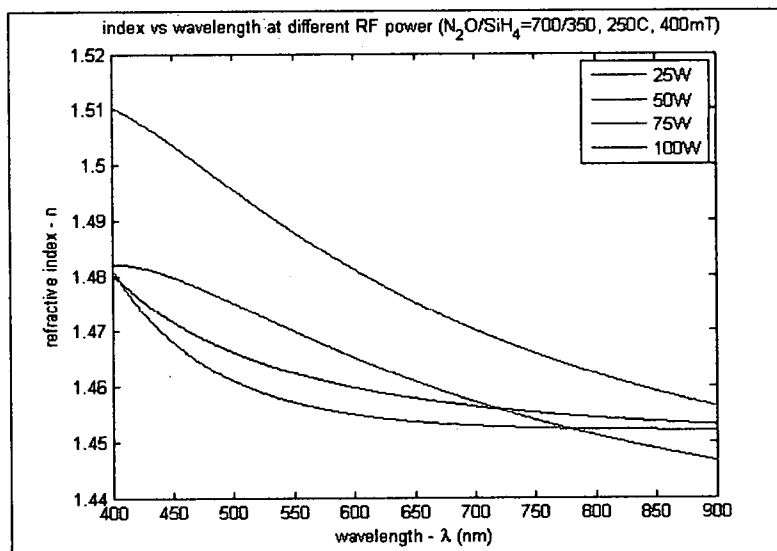


Figure 11 Refractive index of PECVD SiO<sub>2</sub> thin film vs. wavelength at different RF power.

With increasing RF power, the refractive indices were found to decrease. This behavior is due to the higher level of dissociation of N<sub>2</sub>O (which has greater dissociation energy than SiH<sub>4</sub>) under higher RF powers. As the oxygen content in the resultant thin film increases, the overall refractive index becomes lower. Data in Fig. 12 also verifies this observation.

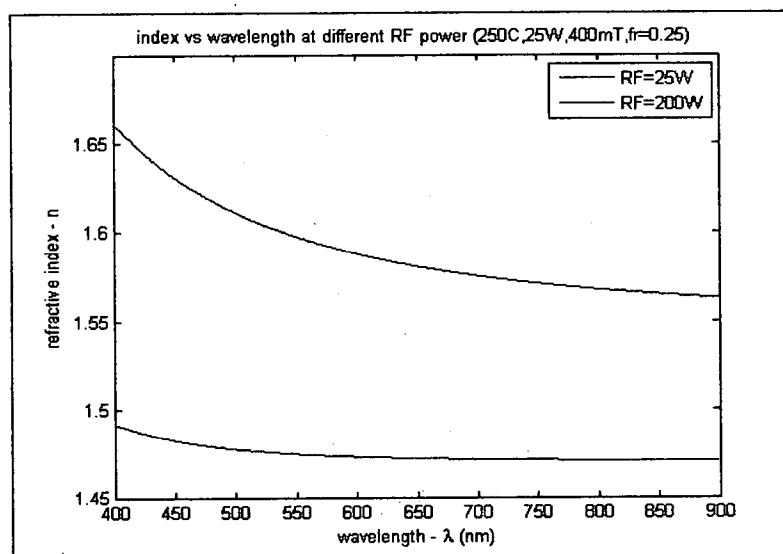


Figure 12 Refractive index of PECVD SiO<sub>2</sub> thin film vs. wavelength at high and low RF power.

At  $\text{N}_2\text{O}/(\text{SiH}_4\&\text{He})$  flow ratio=0.25, samples made under 25W and 200W RF power are compared here. Higher RF power releases more O from  $\text{N}_2\text{O}$  leading to the increased O content in resultant thin film. This explains why the thin films deposited at higher RF powers had lower refractive indices.

Fig. 13 below shows the influence of the RF power on the deposition rate of  $\text{SiO}_2$  thin film deposited by PECVD.

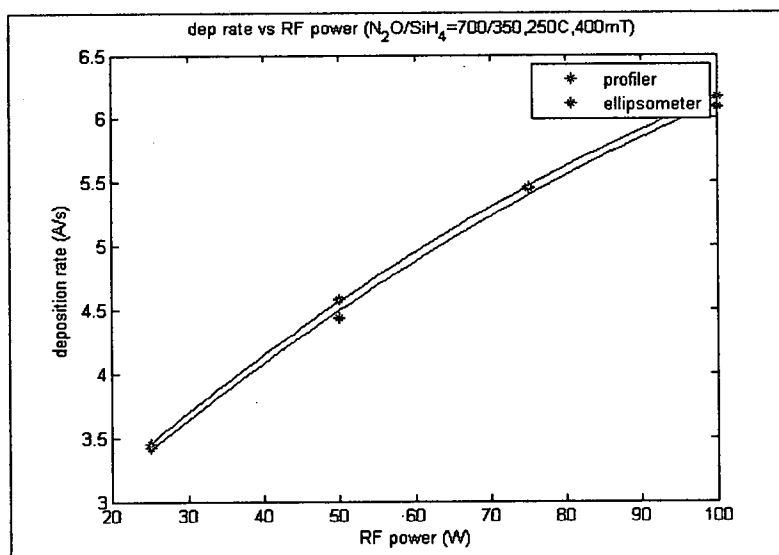


Figure 13 Deposition rate of PECVD  $\text{SiO}_2$  thin film vs. RF power.

The increase in the deposition rate with increasing RF power is as expected. Higher RF power provided more excitation in the plasma to dissociate the bonds of precursor molecules, which made the chemical reaction energetically more favorable. Compared with lower RF power, more moles participated in the chemical reaction under higher RF power, which lead to more deposition in the same period of time, i.e. higher deposition rate is obtained.

### 2.3 Features of Thin Films Deposited by Plasma Enhanced Chemical Vapor Deposition

The main feature of PECVD is its versatility for synthesizing both simple and complex compounds with relative ease at generally lower substrate temperature (compared to non-plasma CVD). Both the chemical composition and physical properties can be tailored by controlling the reaction chemistry and deposition conditions. In  $\text{SiO}_2$  thin films, for example, the ratio between silicon and oxygen can be varied in a large range through control of the source gases flow ratio. The refractive index and the deposition rate are dependent on the process parameters. Thin films deposited by PECVD have a good degree of step-coverage, since the substrate is immersed in the bath of the chemical reaction and the pressure is high (several hundred mT), which leads to short mean free paths. The short mean free path makes the deposition conformal rather than line of sight. The presence of ions bombarding the substrate and thin film produces denser films in PECVD compared to sputtering and evaporation.

### 2.4 Gas Contamination in Plasma Enhanced Chemical Vapor Deposition

After a series of experiments, a small leak in the  $\text{SiH}_4$  gas lines was discovered which lead to the suspicion of gas contamination. Fig. 14 below shows the test results. All four samples are made under exactly the same deposition process conditions ( $\text{N}_2\text{O}$  /( $\text{SiH}_4$ & $\text{He}$ ) flow ratio: 300/100, substrate temperature: 250C, RF power: 25W, process pressure: 400mT), except that the blue line is for direct deposition without any attempts to get rid of gas contamination, the blue dashed is for deposition immediately after the deposition of the blue line, the red line is for deposition after flushing the lines for 5 minutes with the source gases, and the red dashed is for deposition immediately after the

deposition of the red line. We can see that under the same deposition conditions, only the red dashed and the blue dashed have almost the same refractive index. The other two results deviated due to the source gas contamination. We can also see that a 5-minute pre-deposition flush was not enough to entirely get rid of the source gas contamination. The flush time was extended to 10 minutes, but still some contamination. So we just made two samples and used the second ones for measurements in all subsequent results.

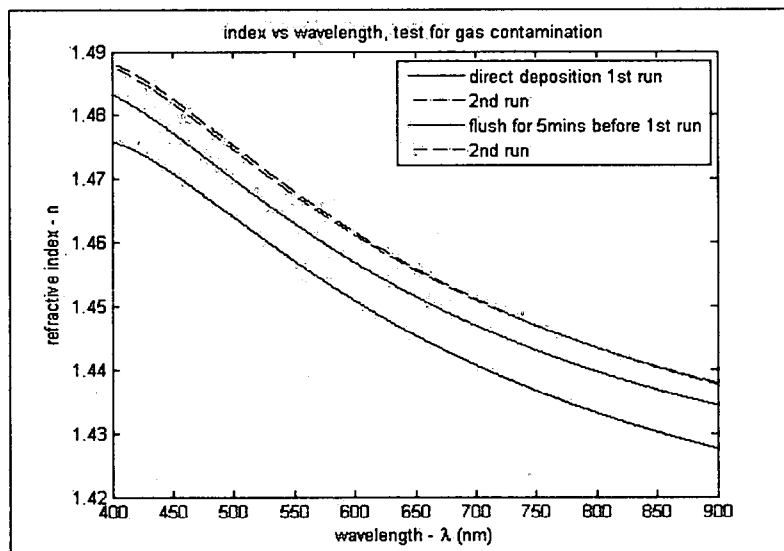


Figure 14 Testing results for gas contamination in PECVD SiO<sub>2</sub> thin film caused by leak in gas lines.

We also noticed that there were some refractive index variations between the samples made immediately after the process parameter change and without any process parameter change. It is because the chamber environment is not stable right after parameter changes. In order to get the most consistent and reliable results, two samples were made in sequence under every process conditions for PECVD, and the second ones were taken for data analysis.

## CHAPTER III

### SiO<sub>2</sub> THIN FILM DEPOSITION USING RF PLASMA SPUTTERING

#### 3.1 Introduction to RF Plasma Sputtering

RF plasma sputtering is a form of high-vacuum physical vapor deposition in which a target material is bombarded by accelerated ions from a gas plasma. The bombardment causes the target atoms to be ejected and creates a layer of thin film on a substrate. RF system is used instead of DC system to sustain the plasma when insulating targets are used. The schematic illustration of the sputtering process is shown in Fig. 15(a).

The RF sputtering tool used for SiO<sub>2</sub> thin film deposition in this thesis is shown in Fig. 15(b). It is a Denton Vacuum Explore 14 model which utilizes Angstrom Sciences magnetron cathodes. It has a 600W RF power supply operating at 13.56MHz [5]. Three cathodes installed in the chamber enable the system to deposit three kinds of materials without opening the chamber. A four-inch rotating stage is used to get good uniformity of the deposition. A quartz crystal monitor is fixed next to the stage to measure the thickness of the thin film deposited on the substrate. The silver or gold coated quartz crystal monitor has reliable and repeatable performance, whose results were confirmed by the measurements on the companion pieces using the profilometer. Companion pieces are small pieces of substrates with several ink (Sharpie™) marks on it, and were put in chamber next to the desired deposition substrate. The marks on the companion pieces can be lifted off in an acetone solvent and an ultrasonic bath after deposition, and the step



height can be measured with the profilometer. The thickness of the thin films deposited by PECVD and evaporator were both measured in the same way.

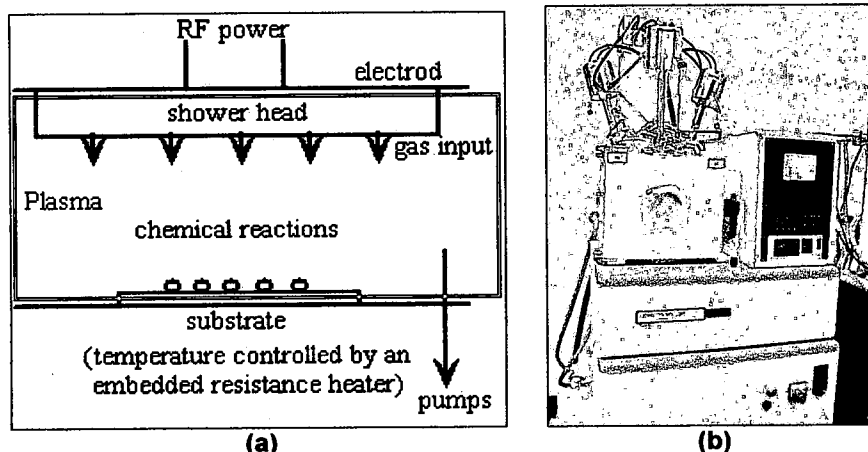


Figure 15 (a) Schematic illustration of RF sputtering. (b) Denton Vacuum RF Sputtering tool.

The photo in Fig. 16(a) shows the Denton chamber in use, the purplish color is Argon plasma. Fig. 16(b) shows  $\text{SiO}_2$  target that was used for the sputtering.

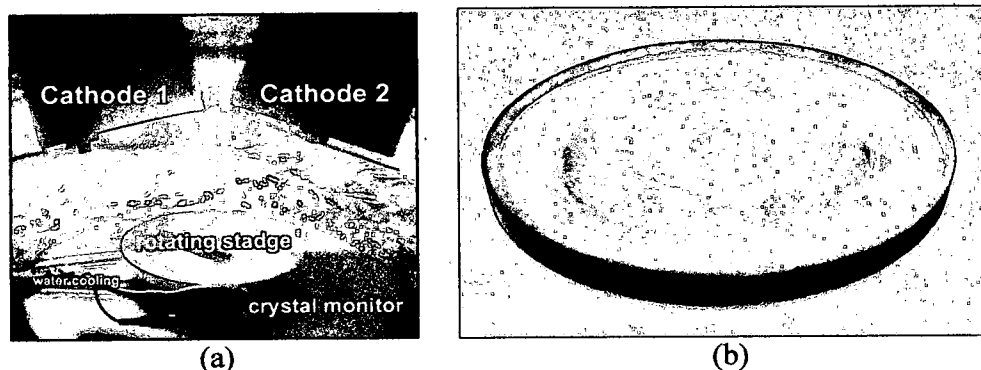


Figure 16 (a) Denton chamber in use. (b)  $\text{SiO}_2$  target for sputtering.

In an RF sputtering system, the RF generator is coupled to the electrode through a DC blocking capacitor. The RF signal will acquire a DC bias because electrons will be captured by the anode faster than secondary electrons can be released through ion bombardment. The magnitude of DC bias depends on the plasma characteristics, the mobility of electron and the rate of secondary electron emission. Generally, lower

background gas pressure and larger RF power result in higher DC bias, which will lead to a higher sputtering rate.

In magnetron sputtering, a magnetic field is used to keep the secondary electrons close to the target surface. Otherwise, they will drift in random directions and produce ions at lower efficiency. The magnetic field created by two concentric ring magnets with opposite polarity causes the secondary electrons to travel in a circular path around the target surface. The magnet configuration is shown in Fig. 17[3]. This increases the electron density at the target surface, leading to more chances of electron-neutral atom collisions and creating more ions. Sputtering rate increases at higher ion density, since more ions are bombarding the target. Because this circular electron path leads to uneven erosion of the target, a characteristic ring pattern on the target is formed, as seen in Fig. 16(b).

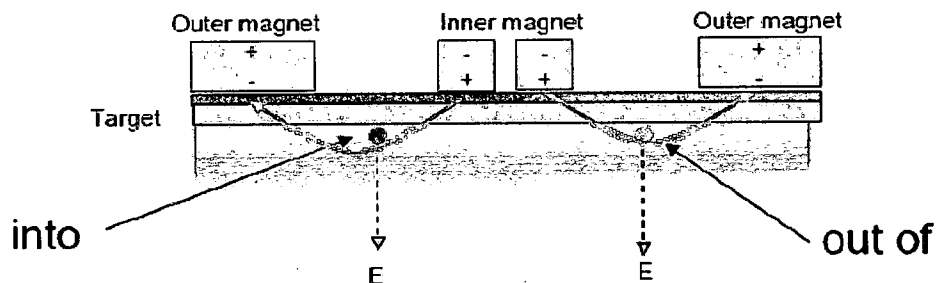


Figure 17 Cross section of the magnet configuration for a magnetron cathode.

Besides sputter deposition, sputtering process can also be used for sputter etching, which is used in the erosion of surfaces, such as patterning semiconductors wafers, cleaning surfaces, micromachining, depth profiling and a number of applications which require careful, microscopic erosion of a surface.

### 3.2 Effects of RF Sputtering Process Parameters on SiO<sub>2</sub> Thin Films

#### 3.2.1 Effects of Process Pressure on SiO<sub>2</sub> Thin Films

Sputtering typically uses a process gas pressure in the mTorr to Torr range. Most magnetrons are best operated at a few mTorr. In addition, due to the reactive nature of many freshly sputtered atom species, the residual or working gas needs to be fairly clean and inert; Argon is used in this thesis. Sputtering systems typically have a base pressure that is several orders of magnitude (at least two) below the operating pressure, and a clean background gas is introduced at the base pressure to bring the pressure up to the process level where plasma can be ignited. All sputtered samples in this thesis were fabricated under the base pressure of 7 $\mu$ Torr to get a good film quality and purity. Refractive index of SiO<sub>2</sub> thin film deposited by RF sputtering as a function of wavelength at different process pressure is shown in Fig. 18 below.

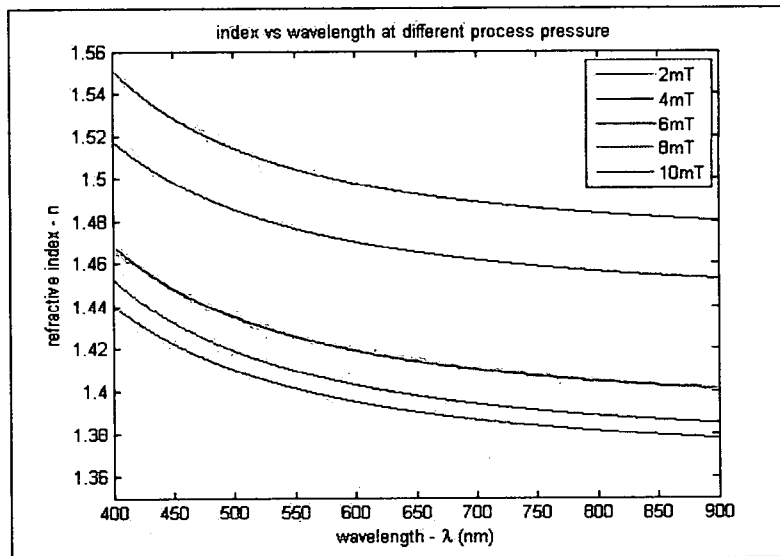


**Figure 18** Refractive index of RF sputtered  $\text{SiO}_2$  thin film vs. wavelength at different process pressure.

With the increasing process pressure, the refractive index first decreased, reached the lowest point at 6mT, and then increased a little. The decrease is probably because at a higher backfill gas pressure, the mean free path will be shorter and the sputtered atoms will have lose most of their momentum when it reached the substrate due to collisions with the gas atoms. The reduced momentum of the atoms leads to a lower density of the thin film. While the increase is probably because that with increasing pressure, DC bias decreases, causing lower sputtering rate. And lower deposition rate tend to form a denser thin film.

Fig. 19 below shows the influences of the process pressure on the deposition rate of  $\text{SiO}_2$  thin film deposited by RF sputtering.

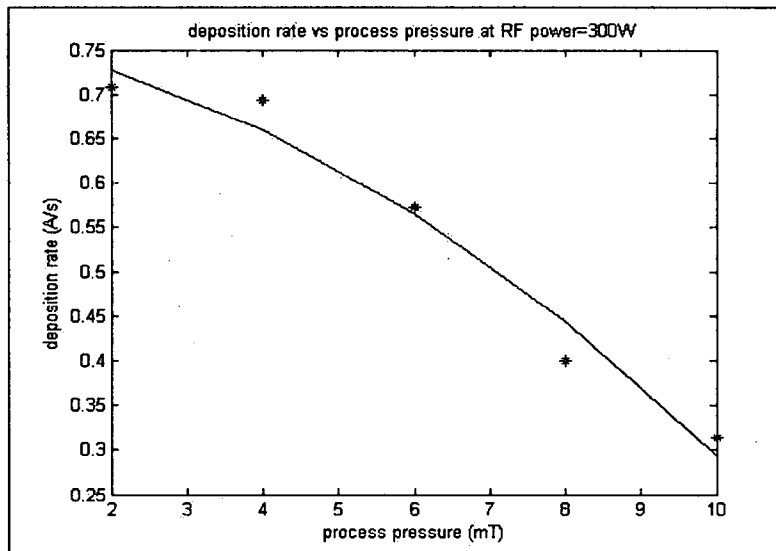


**Figure 19** Deposition rate of RF sputtered SiO<sub>2</sub> thin film vs. process pressure

The decrease in the deposition rate with increasing process pressure is as expected. At higher process pressure, the sputtered atoms are more inclined to be scattered by the background gases, and arrive at the substrate with lower energy and a high oblique component. As a result, a larger surface area will experience deposition leading to greater uniformity. Compared with lower process pressure, the film thickness will be smaller at higher process pressure, i.e. lower deposition rate.

### 3.2.2 Effects of RF Power on SiO<sub>2</sub> Thin Films

RF power is the greatest influence factor on the deposition rate, which is nominally in direct proportion as shown in Fig. 20 below. This is as expected, because more RF power creates more Argon ions, and larger ion acceleration, and more atoms will be dislodged from the target, which lead to a higher deposition rate.

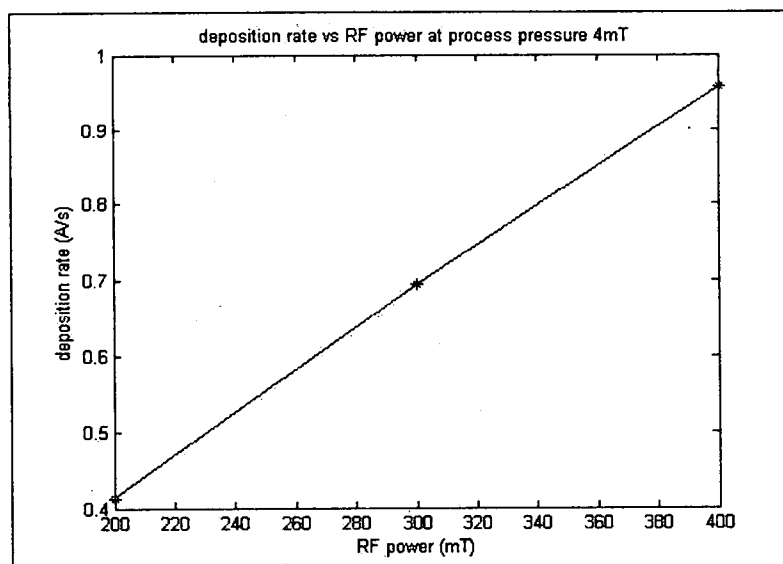
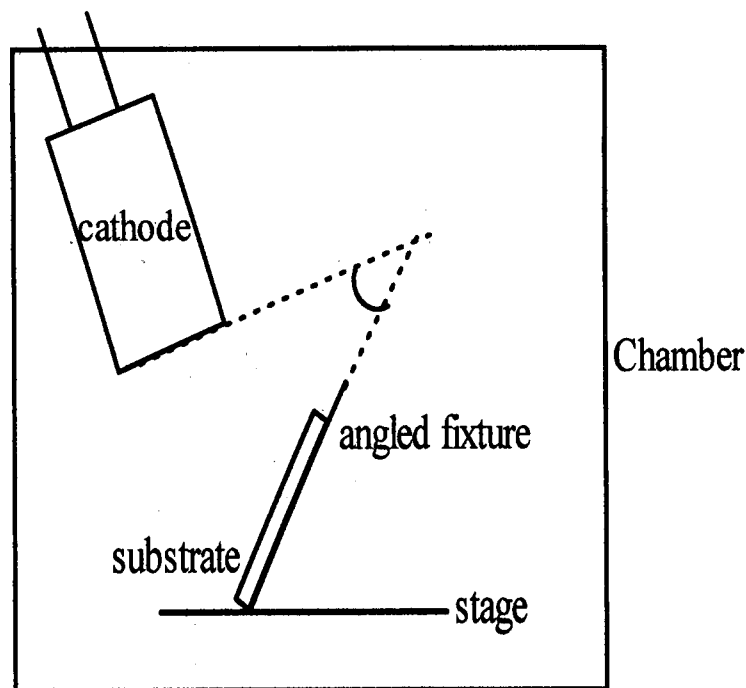


Figure 20 Deposition rate of RF sputtered  $\text{SiO}_2$  thin film vs. RF power.

### 3.2.3 Effects of Sputter Angle on $\text{SiO}_2$ Thin Films

In order to compare with the results of oblique angle E-Beam evaporation, which will be discussed in detail in chapter V, we also sputtered  $\text{SiO}_2$  thin films at oblique angles. However, due to the mechanism of sputtering process, the atoms dislodged from the target were just randomly collected on the substrate rather than organized as nano-rod thin film in oblique angle evaporation. A schematic illustration of the experiment setup is shown below in Fig. 21. The angles were measured between the cathode and the substrate. The stage rotating was disabled, since uniform deposition was not wanted in this case, which would destroy the nano structure if there were any.



**Figure 21** Experiment setup for oblique angle sputtering.

The experimental result is shown below in Fig. 22, which confirms our expectations.

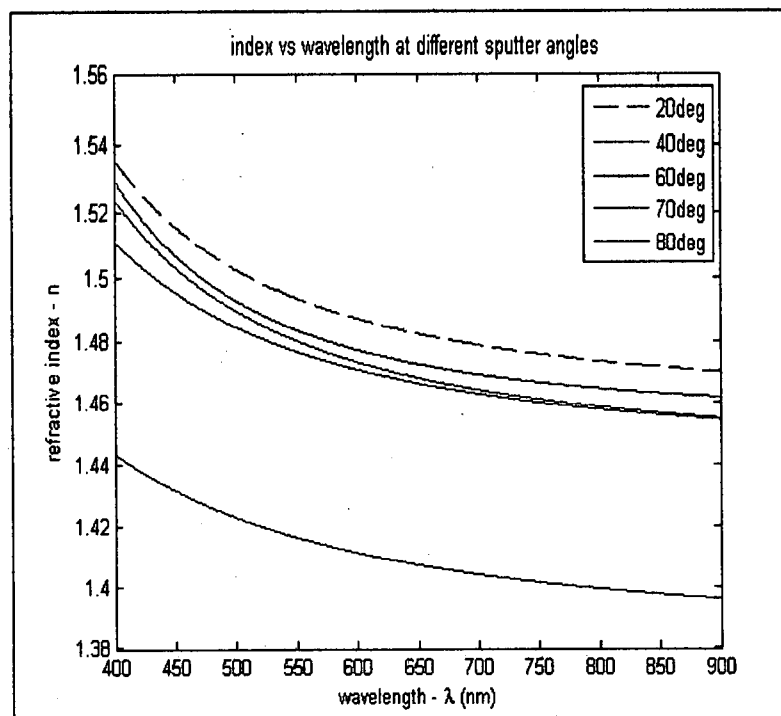


**Figure 22** Refractive index of RF sputtered  $\text{SiO}_2$  thin film vs. wavelength at different sputter angles

In RF sputtering, the refractive index of the deposition is an important indication of porosity. Lower refractive index indicates higher degree of porosity. From the Fig. 22, we can see that the indices of  $\text{SiO}_2$  thin films sputtered at oblique angles from  $20^\circ$  to  $70^\circ$  are all around 1.48 and do not vary much, which indicated that the porosity do not change

much when varying the sputter angle in that range. So there was no sputter angle controlled thin film growth in that range and the products were all solid films. Only at a high sputter degree,  $80^\circ$  here, the refractive index shows an obvious drop. However, this is because of random porosity due to the high oblique sputter angle. No nano-rods structure is exhibited here as seen with E-Beam evaporation.

### 3.3 Features of Thin Films Deposited by RF Sputtering

RF sputtering is widely used for metal, dielectric and semiconductor deposition. Since the target can be kept at a relatively low temperature, it is especially useful for compounds or mixtures, where different components would otherwise tend to evaporate at different rate.

As line-of-sight geometry required in PVD process,  $\text{SiO}_2$  thin films deposited by RF sputtering should be more directional than conformal. However, since the atoms ejected from the target reach the substrate surface with some energy and mobility, there is a random walk motion before they condense on the substrate. As a result, the thin film deposited by sputtering is more conformal than evaporation. The more power the atoms have, and higher the pressure, the more conformal the deposition would be.



## CHAPTER IV

### SiO<sub>2</sub> THIN FILM DEPOSITION USING ELECTRON-BEAM EVAPORATION

#### 4.1 Introduction to Electron-Beam Evaporation

E-Beam evaporation is a type of physical vapor deposition, in which the source material is thermally evaporated in a high vacuum chamber using a high energy electron beam. The electron beam is generated and accelerated to several kV and is focused towards the source ingots to create a liquid melt. Since there is no plasma, and no background gases are used, the vapor leaving the molten source travels in a straight line with a long mean free path and condenses on the substrate surface. The high energy electron beam can be adjusted to be directed at the center surface of the material, limiting the heating to the desired material only and avoiding excessive heating of the crucible to prevent contamination. Fig. 23(a) shows the schematic illustration of the E-Beam evaporation process.

The E-Beam evaporator used for SiO<sub>2</sub> thin film deposition in this thesis is the electron beam system manufactured by Torr International Inc as shown in Fig. 23(b). It consists of electron beam source, vacuum system and process control system.

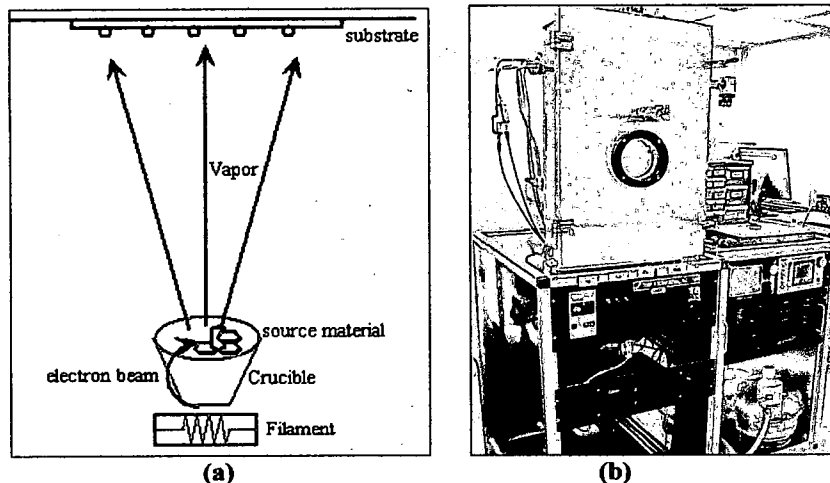


**Figure 23** (a) Schematic illustration of E-Beam evaporation process. (b) International Torr Electron-Beam evaporator.

The electron beam source is a self-accelerated bent beam source. It contains a single filament, four crucible pockets and a 6kW DC power supply [6]. Electrons are originally emitted in all directions by filament, the electron emitter, held at a high negative potential. A beam in a defined direction is formed by the cathode assembly together with the beam former and deflection plate. This beam of electrons is then accelerated through the steep potential gradient formed between the cathode and anode assembly. The culminated beam of high energy electrons is injected into a transverse permanent magnetic field. The magnetic field deflects and focuses the beam through a  $270^\circ$  arc where the beam impacts the material. The impinging electron's kinetic energy is transformed into thermal energy at the impact surface of the source material, while the crucible is water-cooled. Beam sweeping is required to achieve uniform evaporation of subliming vapor, and it is achieved by varying the current supplied to the electro-magnetic coils. These coils provide a time variable deflection of the electron beam along two axes to yield a uniform temperature over a maximum area of the source material [7].

Fig. 24(a) shows the  $\text{SiO}_2$  pellets, which were the source material for  $\text{SiO}_2$  evaporation in this thesis. Fig. 24(b) shows the graphite crucible liner used for  $\text{SiO}_2$  evaporation. Fig. 24(c) shows the crucible with  $\text{SiO}_2$  after evaporation. Unlike many other materials where the pellets completely melt during evaporation,  $\text{SiO}_2$  remains almost the same as solid pellets, and the vapor only occurring through sublimation rather than melting.

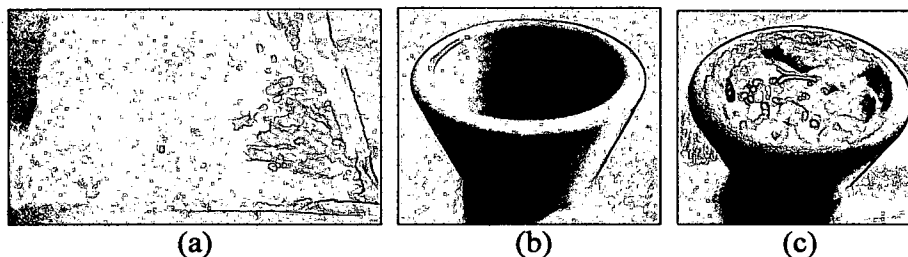


**Figure 24** (a)  $\text{SiO}_2$  source pellets. (b) Graphite crucible used for  $\text{SiO}_2$  evaporation. (c)  $\text{SiO}_2$  in crucible after evaporation.

#### 4.2 Effects of Evaporation Angle on $\text{SiO}_2$ Thin Films

Due to the self-shadowing nature of the evaporation process, the angle of evaporation can affect the porosity of the resultant thin films. Larger evaporation angle will lead to a higher degree of porosity and result in lower refractive index. This will be discussed in detail in 5.3.

#### 4.3 Features of Thin Films Deposited by Electron-Beam Evaporation

Since the E-Beam evaporation is operated under a high vacuum of the order of a few  $\mu\text{T}$ , the vapor leaving the molten source travels in a straight line towards the substrate surface. The evaporated atoms or molecules reach the substrate surface with less energy than in sputtering process. As a result, the film will be highly directional, making the evaporation very useful in creating liftoff structures. Unlike a conformal thin film that

covers all the details of the structure, a directional film leaves the vertical walls open to allow a path for the etching solvents to attack the sacrificial layer.

E-Beam evaporation is widely used for single element materials and every stable compound, such as  $\text{SiO}_2$ . Since the source materials are thermally evaporated, this nature makes the process unsuitable for most compounds. Otherwise, the compound is likely to decompose into its constituent atoms and evaporate at different rate. As a result, the composition of evaporated film can be different from that of the source material.

## CHAPTER V

### ULTRA-LOW REFRACTIVE INDEX NANO-POROUS $\text{SiO}_2$ THIN FILM FABRICATION

#### 5.1 Applications of Ultra-Low Refractive index Nano-Porous $\text{SiO}_2$ Thin Films

The refractive index contrast is a key figure of merit for many applications such as dielectric multilayer structures, optical resonators and photonic crystals. This creates a strong demand for a new class of optical materials that have refractive index much lower than those of conventional materials [8].

The refractive index of the nano-rod  $\text{SiO}_2$  can be made much lower than its bulk counterpart ( $\sim 1.45$ ). Since there are not too many materials with refractive index lower than 1.3, this method enables thin film with optical refractive index as low as 1.05 to be made using standard deposition equipment.

The ultra-low refractive index  $\text{SiO}_2$  thin film combined with other high refractive index material can create a large refractive index contrast. With the ultra-low refractive index that closely matched the refractive index of air, broadband antireflection effect can be achieved by graded-refractive index coatings [9]. This application can be used to improve the extraction efficiency of LED [10].

#### 5.2 Fabrication of Ultra-Low Refractive index Nano-Porous $\text{SiO}_2$ Thin Films

Oblique angle evaporation is a method to grow thin films with a porous microstructure, caused by the self-shadowing nature of the evaporation process. A

random growth fluctuation on the substrate produces shadow regions that the incident vapor flux cannot reach, and a non shadow regions where incident vapor flux deposits preferentially. As a result, an oriented rod like structure is created. The porosity of the nano-rods layer can be adjusted by the incident angle of the vapor flux. In order to get distinct oblique nano-rods, the vapor incident angle has to be fairly large, about  $80^\circ$ . The incident angle of the vapor flux is much larger than the angle of formed oblique nano-rods. Fig. 25 shows the schematic illustration of oblique angle evaporation process.

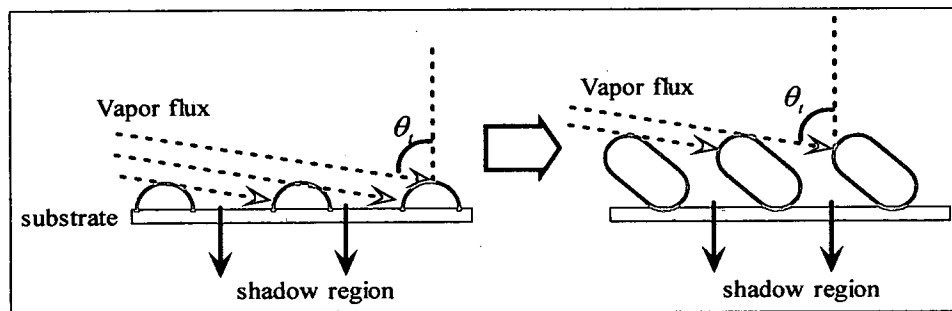


Figure 25 Schematic illustration of oblique angle E-Beam evaporation.

Fig. 26 below shows the experiment setup for the oblique angle E-Beam evaporation. Substrate is placed at an angle, instead of being parallel to the source material as in regular E-Beam evaporation.

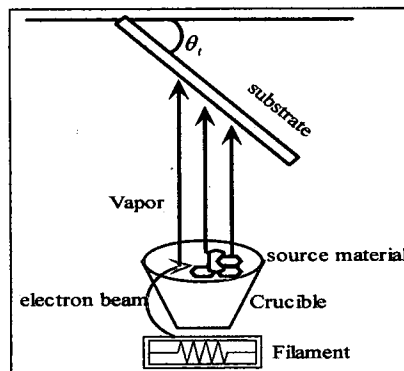
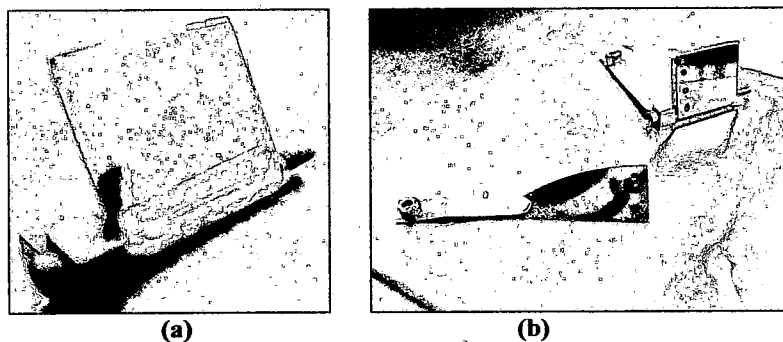


Figure 26 Experiment setup of oblique angle E-Beam evaporation.

An angle adjustable small fixture shown in Fig. 27(a) was machined to hold the substrate in the oblique angle position using high temperature tape (the yellow area). The photo in Fig. 27(b) shows the samples in right position and ready for evaporation. A flat companion piece was used for comparison purpose. Ink marks on the sample pieces were used for thickness measurement by doing lift off after deposition.



**Figure 27** (a) Adjustable angle fixture used in oblique angle evaporation. (b) Samples ready for oblique angle evaporation.

Fig. 28 shows the  $\text{SiO}_2$  nano-rods layer evaporated at flux angle of  $80^\circ$ . The thin film was well organized in a nano-rods fashion. The rods were about 40nm in diameter. The gaps between them were less than 20nm, much smaller than the light wavelength. Thereby, optical scattering is limited.

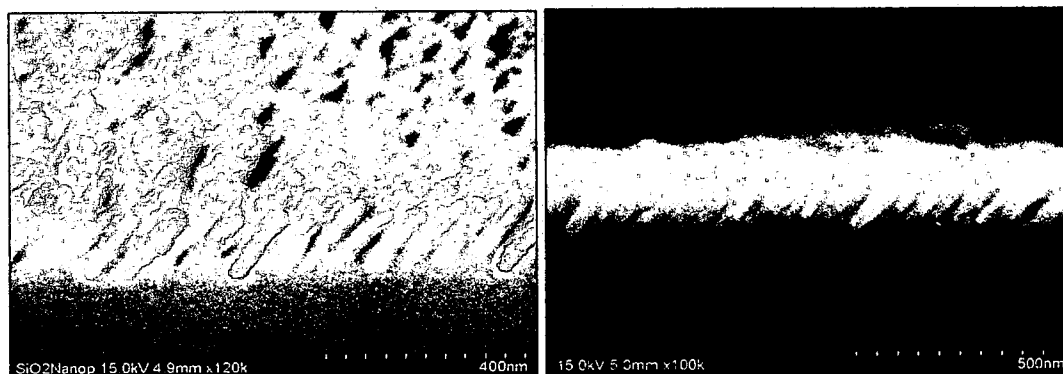


**Figure 28**  $\text{SiO}_2$  nano-rods layer evaporated at  $80^\circ$ .

Besides  $\text{SiO}_2$ , we also tried to evaporate Ti and Ag at an oblique angle. Ti had a similar nano-rods structure as  $\text{SiO}_2$  but with a larger size of 50nm in diameter. The Ti nano-rods layer evaporated at flux angle of  $80^\circ$  are shown in Fig. 29.

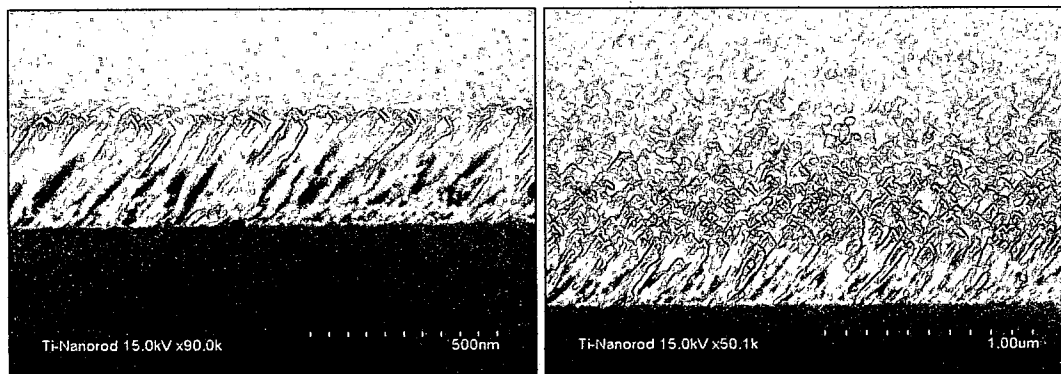
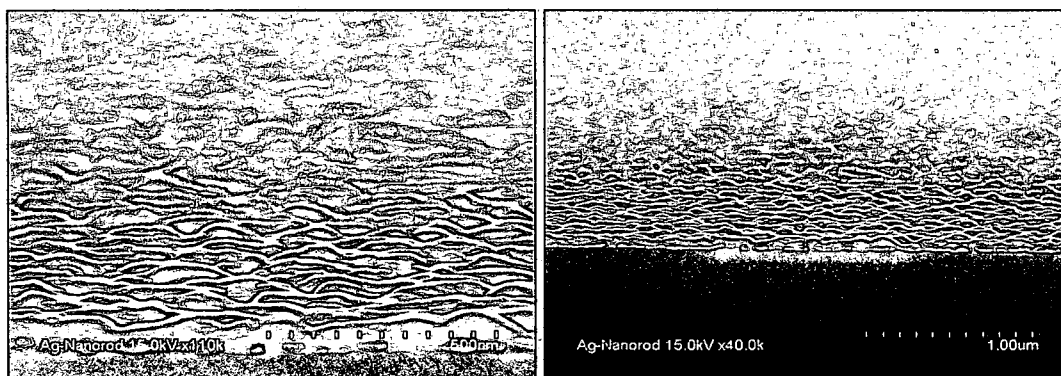


Figure 29 Ti oxide nano-rods layer evaporated at  $80^\circ$ .

The EDX (Energy dispersive X-ray spectroscopy), which is an analytical technique used for the elemental analysis or chemical characterization of a sample, showed that the composition of this nano-rods layer is not only Ti, but Ti and O at 1:1 mol ratio. The O component is caused by oxidization, since the thin film is so porous that superficial oxidization takes place easily in air ambient. So, the incomplete oxidization makes the nano-rods more likely  $\text{TiO}_2$  and Ti mixture, with  $\text{TiO}_2$  around Ti core.

However, for Ag, we didn't get any nano-rods structure at flux angle of  $80^\circ$  as shown in Fig. 30. There were only nano-bumps instead of nano-rods. The reason for this is unclear now. It might be related to material properties of Ag.





**Figure 30** Ag film evaporated at 80°.

When used in multilayer structures, a surface-sealing step is required to prevent the filling of subsequent material into the nano-porous thin film. It can be achieved by evaporating a pore-closure layer. The deposition conditions for the pore-closure layer are almost the same as for the nano-porous layer, except that the vapor flux comes from the opposite direction. Schematic illustration of the process is shown in Fig. 31. In this way, the probability of the subsequent deposition entering the nano-porous film is greatly reduced.

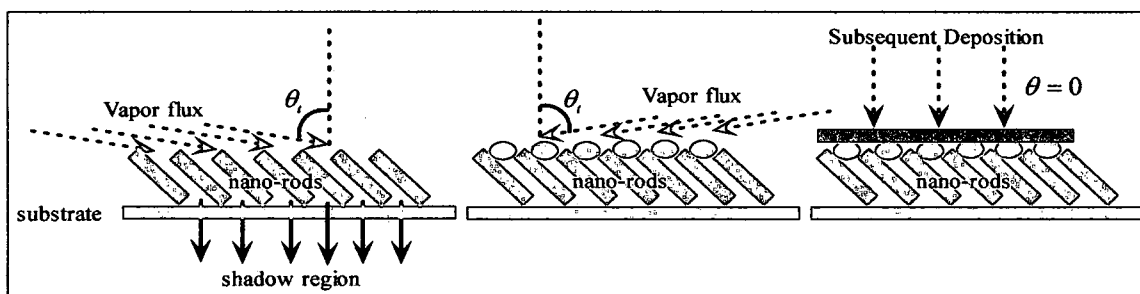


**Figure 31** Surface sealing step in E-Beam oblique angle evaporation.

### 5.3 Effects of Evaporation Angle on Nano-Porous SiO<sub>2</sub> Thin Film

The incident angle of the vapor flux during evaporation can affect the porosity of the nano-rods film. The refractive index of a porous material is determined by the porosity and refractive index of the denser material. The nano-porous SiO<sub>2</sub> thin film consists of

SiO<sub>2</sub> nano-rods and air gaps, so its refractive index should be lower than the refractive index of SiO<sub>2</sub>, which is around 1.45, and higher than the refractive index of air, which is approximately 1, and can be anywhere in between.

Fig. 32 below shows the influence of E-Beam evaporation angle on the SiO<sub>2</sub> thin film refractive index. The angles were measured between the source material plane and the substrate plane.

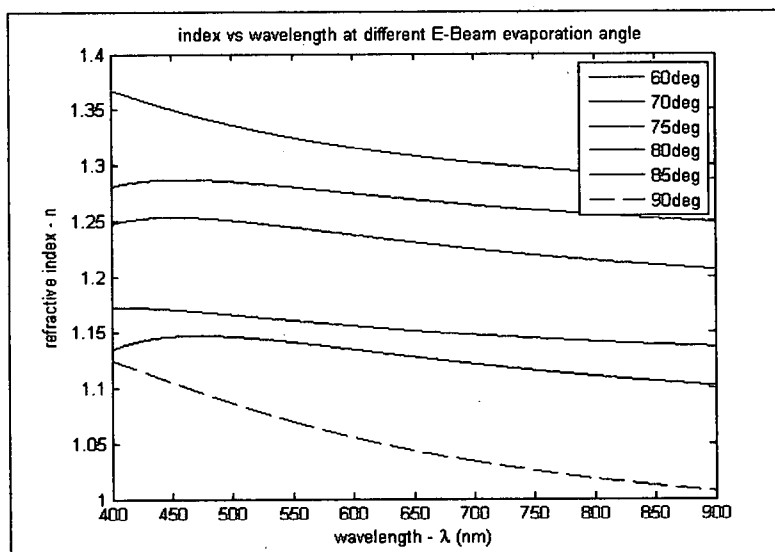
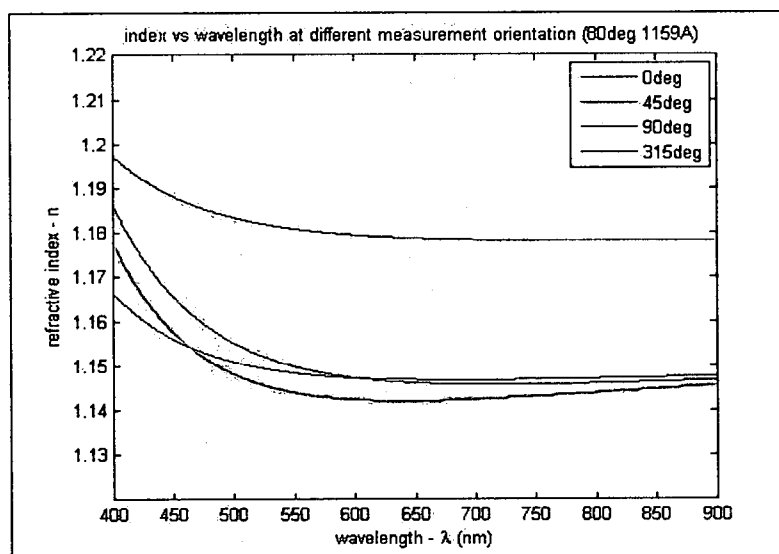


Figure 32 Refractive index of E-Beam evaporated SiO<sub>2</sub> thin film vs. wavelength at different evaporation angle

With increasing evaporation angle, the SiO<sub>2</sub> thin film refractive index consistently drops. Refractive index of SiO<sub>2</sub> thin film reached as low as 1.05. This behavior is as expected, because higher incident angle results in larger shadow regions, which leads to higher porosity of the thin film. As a result, refractive index decrement was observed.

There should be birefringence phenomena for a thin film structured in aligned nano-rods fashion. In order to prove our expectation, we measured the sample at different orientations, refractive index results were compared in the Fig. 33 below. The legend describes the sample orientations with respect to the incident plane during the

measurement, where  $90^\circ$  was the sample position that the ellipsometer incident beam came aligned along the nano-rods growth direction, and  $0^\circ$ ,  $45^\circ$  and  $315^\circ$  were all the samples positions that the incident beam came at an angle with respect to the nano-rods growth direction. The refractive index difference between these two cases is distinct, while the refractive index measured at  $0^\circ$ ,  $45^\circ$  and  $315^\circ$  positions were relatively close. This can be best explained by the birefringence of the nano-rods thin film. The refractive index measured at  $90^\circ$  position is  $n_e$ , and indices measured at other three positions are  $n_o$ . The index difference between these two cases can be roughly seen as the difference between  $n_e$  and  $n_o$ . For more accurate accounting of the birefringence of the nano-porous film, techniques such as generalized ellipsometry will be necessary, which is beyond the scope of the current study [11].



**Figure 33** Refractive index of E-Beam evaporated SiO<sub>2</sub> thin film vs. wavelength at different measurement orientations.

## CHAPTER VI

### ELLIPSOMETRY

#### 6.1 Introduction to Ellipsometry

The thin films samples described above were characterized with variable angle spectroscopic ellipsometer. Ellipsometry is a sensitive and powerful optical technique for the investigation of the dielectric properties of thin films using polarized light. It has applications in many different fields, from basic scientific research to industrial applications. As an optical technique, ellipsometry is inherent non-destructive and contactless. It derives its sensitivity, which is greater than a simple reflectance measurement, from the determination of the relative phase changes between two orthogonal polarization components of a polarized light beam reflected off the sample and no absolute intensity of the reflected light measurements are needed [12].

Ellipsometer measures the change in polarization state of light reflected from the surface of a sample. The typical measured quantities are expressed as  $\Psi$  and  $\Delta$  pair, which are related to the ratio of Fresnel reflection coefficients  $r_p$  and  $r_s$  for p and s polarized light respectively [13]:

$$\rho = \frac{r_p}{r_s} = \tan\Psi \exp(i\Delta) \quad (10)$$

Because ellipsometer measures the ratio of two reflection coefficients, it can be highly accurate and very reproducible. The ratio is complex number containing phase information:  $\Delta$ , which makes the measurements very sensitive [14].

## 6.2 SiO<sub>2</sub> Characterization Using Ellipsometry

PhE-102 Spectroscopic Ellipsometer manufactured by Angstrom Advanced Inc. was used to measure the refractive indices and thicknesses of the samples in this thesis. It is a computer controlled high precision measuring instrument consisting of a spectroscopic ellipsometer hardware, a control box and a PC computer, as shown in Fig. 34 below. The ellipsometer consists of incident and exit arms used for measuring the change in polarization state, a laser used to align sample, a sample stage, and a goniometer to adjust measurement angle.

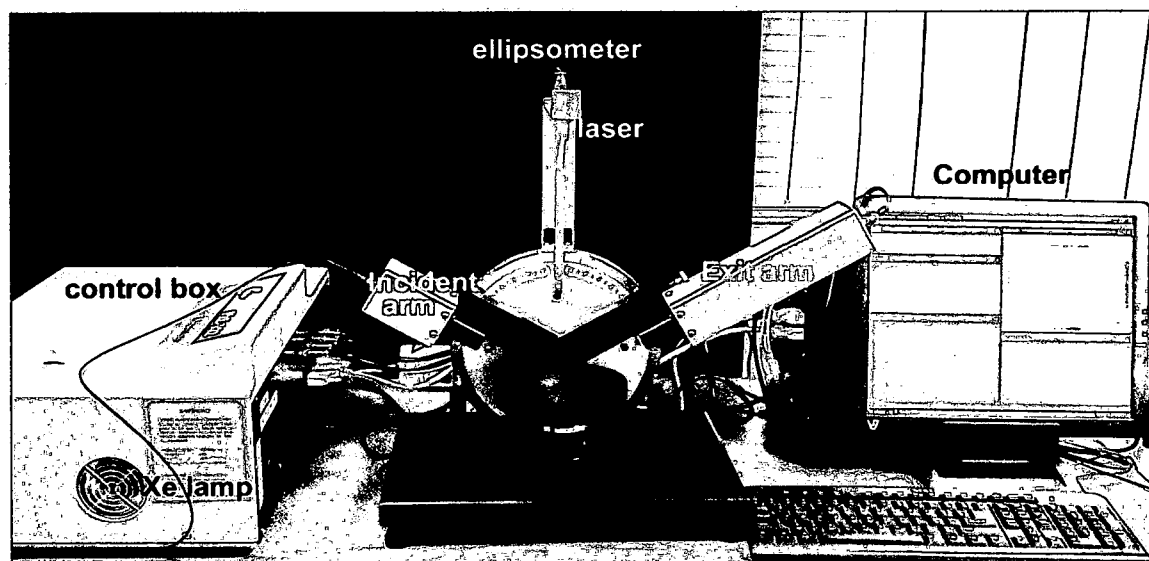


Figure 34 PhE-102 spectroscopic Ellipsometer.

The combination of variable angle of incidence and spectroscopic measurements allows the user to acquire large amounts of data from a given sample and the flexibility necessary to handle a very broad range of sample materials and structures. The thicknesses and refractive indices of SiO<sub>2</sub> thin films on silicon substrates were measured

with ellipsometer using the incident angles of 60° and 70°. Better fittings were obtained at 60°.

The light source of the ellipsometer is Xe lamp, the wavelength of which ranges from 250nm to 1700nm. However, only the 400nm to 900nm wavelength range were investigated for the SiO<sub>2</sub> films on silicon substrates, because 1100nm is the cutoff wavelength for the silicon detector used in the ellipsometer detection arm and the measurement close to the cutoff wavelength would not be very reliable.

A “Cauchy layer on Si substrate” was used as the ellipsometry model and found to fit the measurement data very well. An example of the  $\Psi$  and  $\Delta$  fittings are given in Fig. 35 below. The experiment data and the generated data matched to each other very well, which indicates the results obtained were very accurate.

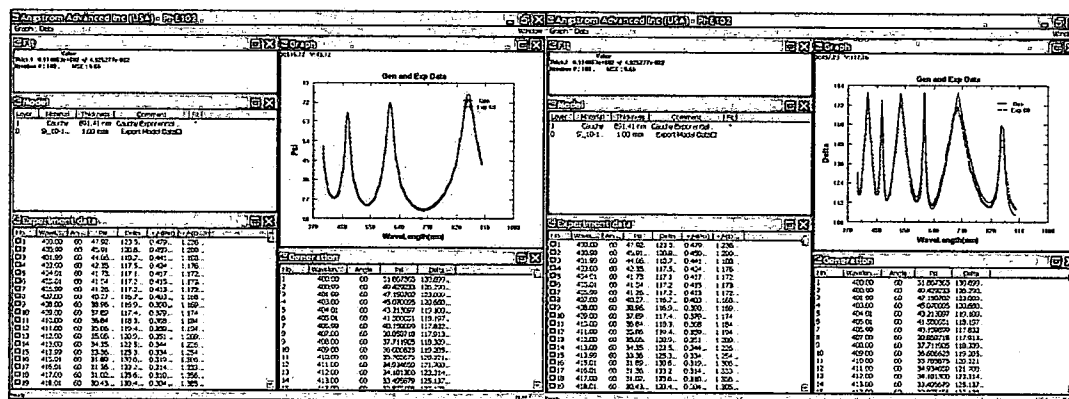


Figure 35 Ellipsometer fitting curves of  $\Psi$  and  $\Delta$ .

It is necessary to specify the refractive index of the silicon substrate in the optical model to be used by the fitting algorithm. The silicon substrate data used for the fitting was obtained from measuring our own silicon substrate actually used for the deposition with the same spectroscopic ellipsometer instead of using existing default data in file. This provided us with better fittings and more accurate results.

Ellipsometry has played a crucial role in the development of  $\text{SiO}_2$  and other thin films used in microelectronics, and it has also had a major role as a general method for various thin film characterization.

## CHAPTER VII

### CONCLUSIONS

A wide variety of processing technologies are available for the deposition of thin films. The technologies differ to a large degree in their physical and chemical principles of operation and in the commercially available types of equipment. Each processing technology has been pursued or developed because it has unique advantages over others. However, each processing technology has its limitations. In order to optimize the desired film characteristics, a good understanding of the process control and the advantages and restrictions applicable to each technology is necessary.

Three common methods to deposit  $\text{SiO}_2$  thin films on silicon substrates were investigated in order to have a better understanding of how processing parameters can affect thin film properties, especially the refractive index and the deposition rate. The deposition of a novel ultra-low refractive index nano-porous  $\text{SiO}_2$  thin film was demonstrated using oblique angle E-Beam Evaporation. Birefringence of a thin film structured in such aligned nano-rods fashion was expected and proved. Future research can focus on characterization of the anisotropy of this nano-porous thin film, using generalized ellipsometry.



R002593952

## BIBLIOGRAPHY

- [1] Smith, Donald L. Thin-film deposition: principles and practice. New York: McGraw-Hill, 1995.
- [2] Seshan, Krishna. Handbook of thin-film deposition processes and techniques: principles, methods, equipment and applications. Norwich, N.Y.: Noyes Publications/William Andrew Pub., 2002.
- [3] Sarangan, Andrew M. "Nano-Fabrication." [class notes], EOP 695 (2008).
- [4] Unaxis USA Inc. "790 Series Plasma Processing System User Manual."
- [5] Denton Vacuum, LLC. "Denton Vacuum Explorer 14 Operating Manual."
- [6] Torr International Inc. "Electron Beam System manual." Model No. EB-4P-6KW, Serial No. EBES-DYOH-MN4.
- [7]MDC Vacuum Products Corp. "Electron Beam Evaporation Source." (April 2002).
- [8] Xi, J.-Q., Jong Kyu Kim, and E. F. Schubert. "Low-Refractive-Index Films: A New Class of Optical Materials." IEEE LEOS Newsletter (December 2005).
- [9] Xi, J.-Q. et al. "Optical thin-film materials with low refractive index for broadband elimination of Fresnel reflection." Nature Photonics 1, (March 2007): 176-179.
- [10] Kim, J.K. et al. "GaInN light-emitting diode with conductive omnidirectional reflection having a low-refractive-index indium-tin oxide layer." Appl. Phys. Lett. 88, 013501 (2006).
- [11] Azzam, R.M.A and N.M. Bashara. "Application of Generalized ellipsometry to anisotropic crystals." J. Opt. Soc. Am. 64, no. 2 (1974):128-133.
- [12] Harland G. Tompkins and Eugene A. Irene. Handbook of ellipsometry. Norwich, NY: William Andrew Pub.; Heidelberg, Germany: Springer, 2005.
- [13] Zhan, Qiwen. "Polarization of Light." [class notes], EOP 665 (2008).
- [14] Angstrom Advanced Inc. "PhE-102 Spectroscopic Ellipsometer Manual."